[redacted]

[redacted]

Copy 223
RM L56F26

TECH LIBRARY KAFB, NM
0144212

NACA RM L56F26

7708

Rg # 1723

NACA

RESEARCH MEMORANDUM

MEASUREMENTS OF AERODYNAMIC HEAT TRANSFER AND BOUNDARY-LAYER TRANSITION ON A 15° CONE IN FREE FLIGHT AT SUPERSONIC MACH NUMBERS UP TO 5.2

By Charles B. Rumsey and Dorothy B. Lee

Langley Aeronautical Laboratory
Langley Field, Va.

[redacted]

[redacted] the meaning of [redacted] U.S.C., Secs. 793 and 794, the transmission or revelation of which [redacted] any [redacted]

NATIONAL ADVISORY COMMITTEE FOR AERONAUTICS

WASHINGTON

October 15, 1956

[redacted]

TECH LIBRARY KAFB, NM

0144212

NATIONAL ADVISORY COMMITTEE FOR AERONAUTICS

RESEARCH MEMORANDUM

MEASUREMENTS OF AERODYNAMIC HEAT TRANSFER AND BOUNDARY-LAYER TRANSITION ON A 15° CONE IN FREE FLIGHT AT SUPERSONIC MACH NUMBERS UP TO 5.2

By Charles B. Rumsey and Dorothy B. Lee

SUMMARY

Measurements of aerodynamic heat transfer have been made at several stations on the 15° total angle conical nose of a rocket-propelled model in free flight at Mach numbers up to 5.2. Data are presented for a range of local Mach number just outside the boundary layer from 1.40 to 4.65 and a range of local Reynolds number from 3.8×10^6 to 46.5×10^6, based on length from the nose tip to a measurement station.

Laminar, transitional, and turbulent heat-transfer coefficients were measured. The laminar data were in agreement with laminar theory for cones, and the turbulent data agreed well with turbulent theory for cones using Reynolds number based on length from the nose tip.

At a nearly constant ratio of wall to local static temperature of 1.2, the Reynolds number of transition increased from 14×10^6 to 30×10^6 as Mach number increased from 1.4 to 2.9 and then decreased to 17×10^6 as Mach number increased to 3.7.

At Mach numbers near 3.5, transition Reynolds numbers appeared to be independent of skin temperature at skin temperatures very cold with respect to adiabatic wall temperature.

The transition Reynolds number was 17.7×10^6 at a condition of Mach number and ratio of wall to local static temperature near that for which three-dimensional disturbance theory has been evaluated and has predicted laminar boundary-layer stability to very high Reynolds numbers ($\sim 10^{12}$).

INTRODUCTION

A program for the investigation of aerodynamic heat transfer and boundary-layer transition on bodies in free flight at high supersonic speeds is being conducted by the Langley Pilotless Aircraft Research Division. The first results of this program were measurements of turbulent heat transfer at single points on a parabolic nose and on two 10° total angle conical noses at Mach numbers near 4 (refs. 1 and 2) and on a modified von Kármán nose shape tested to Mach number 10.4 (ref. 3).

After the development of a system for commutating and telemetering thermocouple measurements of skin temperature at several points on a body, laminar and turbulent heat-transfer data were measured at six stations on a parabolic body (NACA RM-10) at Mach numbers up to 4.2 (ref. 4), and on a 10° total angle conical nose at Mach numbers up to about 5 (ref. 5).

The purpose of the present test was to investigate the heat transfer and location of transition on a sharp 15° total angle cone at Mach numbers up to 7, by means of skin-temperature measurements at several stations along the conical nose of a three-stage rocket-propelled model. Because of a partial telemeter failure, skin-temperature data ended at a time about half way through burning of the final propulsion stage, that is, at a Mach number of 5.2. Other telemetered data were obtained until a short time after the peak Mach number of 7.3.

Skin-temperature measurements were obtained at nine stations along the 31-inch nose of the model. Laminar, turbulent, and transitional heat-transfer data and transition Reynolds numbers were measured during the test which covered a range of local Mach number just outside the boundary layer on the cone from 1.40 to 4.65 and a range of local Reynolds numbers based on length from the nose tip to a measurement station from 3.8×10^6 to 46.5×10^6.

The flight tests were conducted at the Langley Pilotless Aircraft Research Station at Wallops Island, Va.

SYMBOLS

A area, sq ft

c_f local skin friction coefficient

C_H Stanton number, $\dfrac{h}{gC_p\rho_v V_v}$

C_p	specific heat of air at constant pressure, Btu/lb-°F
C_w	specific heat of wall material, Btu/lb-°F
g	gravitational constant, 32.2 ft/sec^2
h	local aerodynamic heat-transfer coefficient, Btu/ft^2-sec-°F
J	mechanical equivalent of heat, ft-lb/Btu
K	thermal conductivity of air, Btu-ft/ft^2-sec-°F
K_w	thermal conductivity of wall material, Btu-ft/ft^2-sec-°F
M	Mach number
Pr	Prandtl number, $gC_p\mu/K$
Q	quantity of heat, Btu
R	Reynolds number, $\rho VX/\mu$
R.F.	recovery factor $= \dfrac{T_{aw} - T_v}{T_{so} - T_v}$
T	temperature, °R, except as noted
t	time, sec
V	velocity, ft/sec
X	distance along nose surface from tip, ft
β	Stefan-Boltzman constant, 4.8×10^{-13} Btu/sec-ft^2-°R^4
ϵ	ratio of emissivity of skin to emissivity of a black body
ρ	density of air, slugs/cu ft
ρ_w	density of wall material, lb/cu ft
τ	thickness of wall, ft
μ	viscosity of air, slugs/ft-sec

Subscripts:

aw	adiabatic wall
o	undisturbed free stream ahead of model
so	stagnation
v	local condition just outside the boundary layer
w	wall
tr	condition at beginning of transition

MODEL AND TESTS

The model was a body of revolution $7\frac{1}{6}$ feet long with a conical nose, a cylindrical midsection, and conical flare rearward section. Figure 1(a) is a photograph of the model, and pertinent dimensions are given in figure 1(b). The 15° total angle conical nose was 31 inches long and consisted of a spun Inconel skin approximately 0.027 inch thick with a stainless-steel tip, hollowed out as indicated in figure 1(b) and welded to the conical skin. The radius of the point of the nose tip was approximately 0.010 inch. The exterior surface of the entire nose was highly polished and the surface roughness, as measured by a Physicists Research Company profilometer, was from 6 to 10 microinches root mean square. The 8.5-inch-diameter cylindrical section and the 10° half-angle conical flare were made of rolled Inconel. The flare skin was backed by balsa wood to maintain its shape.

Two channels, 3/4 inch wide by 1/4 inch high, were located externally on opposite sides of the cylindrical part of the body to provide cable conduits from the telemeter in the nose of the model to the base of the flare where the power plugs and antenna were located.

The propulsion system consisted of two booster stages, each being an M-5 JATO rocket motor, and a T-40 sustainer motor. Because the sustainer motor was to fire at high altitude, it was equipped with a special nozzle designed to expand the exhaust gases to the static pressure for 50,000 feet altitude. A photograph of the model-booster combination on the launcher is shown in figure 1(c).

The model was launched at an elevation angle of 70°. The first booster accelerated the combination to a Mach number of 1.47, where it drag separated at burnout. The second-stage booster and the model, which were locked together, coasted upwards for a predetermined time until the second-stage booster ignited and accelerated them to a Mach number of 4.2.

After a three-second coasting period, the sustainer motor fired and its blast caused disengagement of the second-stage booster. The sustainer motor accelerated the model to a Mach number of 7.2.

During the test, skin temperatures along the conical nose were measured by means of thermocouples at points 6.5, 9.5, 11, 12.5, 14, 15.5, 17, 25, and 29 inches from the nose tip. (Thermocouples located at 8 inches and 21 inches failed to record.) The thermocouples were no. 30 chromel alumel wire and were spot welded to the inside surface of the skin at the measurement stations. The thermocouple readings and three reference voltages (supplied by mercury cells) were commutated and transmitted by the telemeter in the nose of the model. The commutation rate was such that the temperature at each station was recorded every 0.2 second. The three reference voltages, also recorded every 0.2 second, were chosen equivalent to zero scale, half scale, and full scale of the thermocouple temperature range, and thus supplied an inflight check for the calibration of the temperature measurement system.

Thrust and drag acceleration were also telemetered, and although the telemeter channel carrying the temperature measurements stopped transmitting during firing of the sustainer motor, the accelerometer channels continued to transmit until a time shortly after burnout of the sustainer motor.

Velocity data were obtained by means of CW Doppler radar and the altitude and flight-path data were measured by an NACA modified SCR 584 tracking radar. The model went out of range of the CW Doppler radar just before burnout of the sustainer motor, and Doppler velocity data were extended to the time of telemeter failure by integration of the telemetered acceleration. Atmospheric and wind conditions were measured by means of radiosondes launched near the time of flight and tracked by an AN/GMD-1A Rawin set.

Figure 2 shows time histories of the flight Mach number and the free-stream Reynolds number per foot. The variation of altitude with time is shown in figure 3.

DATA REDUCTION

The time rate of change of heat within the skin at a given station on the conical nose can be written

$$\frac{dQ}{dt} = \rho_w \tau C_w A \frac{dT_w}{dt}$$

$$= hA\left(T_{aw} - T_w\right) - A\beta\epsilon T_w^4 + AK_w\tau\left[\frac{\partial^2 T_w}{\partial X^2} + \frac{1}{X}\frac{\partial T_w}{\partial X}\right] \qquad (1)$$

This equation neglects heat absorbed by the skin from solar radiation and heat radiated by the skin to the inner radiation shield. Estimates show that each of these factors is negligible for the test conditions and, furthermore, their effects on the determination of the heat-transfer coefficient are compensating.

The last term on the right-hand side of equation (1) represents the heat flow due to conduction along the skin. Computation showed that the effect of conduction on the aerodynamic heat-transfer coefficient was always less than 2 percent (generally much less); therefore, the last term was disregarded.

The expression for the aerodynamic heat-transfer coefficient is then

$$h = \frac{\rho_w \tau C_w \frac{dT_w}{dt} + \beta \epsilon T_w^4}{T_{aw} - T_w} \tag{2}$$

Experimental values of h were determined at each station for several times during the test by using the measured skin temperature T_w and the rate of change of skin temperature with time dT_w/dt in equation (2). Other parameters in the equation were determined as follows.

The skin thicknesses τ were measured at each station and the density of Inconel, ρ_w, was known. The variation of C_w, the specific heat of Inconel, is given in reference 1 for the temperature range 30° F to 930° F. The emissivity ϵ was considered to be 0.3, since reference 6 shows that for unoxidized Inconel the emissivity varies only slightly from this value for the present range of skin temperature. It may be noted that the radiation term in equation (2) contributed less than 5 percent of the total value in the determination of h in most cases, and less than 15 percent in all cases. The adiabatic wall temperature T_{aw} was obtained from the relation

$$T_{aw} = R.F.\left(T_{so} - T_v\right) + T_v \tag{3}$$

with recovery factor equal to $Pr^{1/3}$ for turbulent flow and to $Pr^{1/2}$ for laminar flow with Pr evaluated at wall temperature. T_v was obtained from the conical-flow tables (ref. 7) with cone angle and free-stream temperature and Mach number known. The stagnation temperature T_{so} was determined from the energy equation

$$\frac{V^2}{2Jg} = \int_{T_o}^{T_{so}} C_p \, dT \tag{4}$$

Values of the integral in equation (4) were obtained from table I of reference 8.

After h had been determined, the Stanton number, based on local conditions just outside the boundary layer, was calculated from

$$C_H = \frac{h}{gC_p\rho_V V_V} \tag{5}$$

The specific heat of air at T_V was obtained from reference 9. Values of ρ_V and M_V were determined from the conical-flow tables (ref. 7) with the cone angle and free-stream conditions known; values of V_V were computed from M_V and T_V.

RESULTS AND DISCUSSION

Skin Temperature Time Histories

Skin temperatures measured at the forward station (6.5 inches from the nose tip) and at the rearmost station (29.0 inches from the nose tip) are shown in figure 4(a). Prior to 14.3 seconds, when the second-stage booster fired, the changes in skin temperature were small; but after this time, the skin temperature at both stations increased rapidly as the Mach number increased. The heating rates decreased somewhat during the coasting period between 17.7 seconds and 20.5 seconds, but increased again when the sustainer motor fired at 20.5 seconds. The large difference in the maximum temperatures at stations 6.5 and 29 indicates different types of boundary layer at the two stations as will be noted later from the heat-transfer coefficients. Figure 4(b) shows the temperature time histories of all the measurement stations during the period of strong aerodynamic heating and high Mach number from 15 seconds until the thermocouple telemeter failed. The temperatures at stations 9.5 and 11.0 were lower than at station 6.5, but at the further rearward stations the temperatures were progressively higher. At the two most rearward stations (25 and 29), the temperatures were similar. The rather sharp changes in slope of the curves for the intermediate stations indicate changes from laminar to

turbulent boundary layer or vice versa. The character of the boundary layer and the location of transition can be determined best from the heat-transfer coefficients and will be discussed subsequently.

Heat Transfer

Local heat-transfer coefficients in the form of Stanton number were reduced from the skin temperature time histories as described in the section on "Data Reduction" for several times during the high Mach number portion of the flight after 15 seconds. Heat-transfer data were not reduced for times prior to 15 seconds because of the low heating rates as mentioned previously. Figures 5(a) to 5(i) show the values of C_H obtained at stations 6.5, 9.5, 11.0, 12.5, 14.0, 15.5, 17.0, 25.0, and 29, respectively. The data are plotted against time because Mach number, Reynolds number, and the ratio of wall temperature to local static temperature all vary simultaneously during the test; thus it was impossible to isolate their individual effects on C_H. The variation of these parameters, M_V, R_V (based on length from the nose tip to the measurement station), and the temperature ratio T_w/T_V are plotted for each station, against the same time scale as the experimental values of C_H. The local Mach number is identical for each station but is repeated on each figure for convenience.

For comparison with the experimental C_H data, theoretical values of laminar C_H and of turbulent C_H for the test conditions are also plotted. The theoretical laminar values were obtained from the flat-plate theory of reference 10, multiplied by $\sqrt{3}$ to convert to conical values. The theoretical turbulent values of C_H were determined by first obtaining values of c_f for a cone using the turbulent flat-plate theory of reference 11 and the method of reference 12 to convert to conical flow. The flat-plate theory of reference 11 was used in the form assuming the von Kármán mixing length law as suggested on page 16 of reference 13. The cone values of c_f were converted to C_H by the relation $C_H = 0.6c_f$ according to reference 14. It is to be noted that this theoretical prediction of turbulent C_H on a cone assumes turbulent boundary layer from the nose tip.

The time histories of experimental C_H for stations 6.5, 9.5, and 11 (figs. 5(a), 5(b), and 5(c)) show that the boundary layer was continuously laminar at these stations during the test period from 15.0 seconds to 23.4 seconds. During this time, the local Mach number varied from 1.42 to 4.65, the local Reynolds number varied from 4×10^6 (minimum for station 6.5) to 18×10^6 (maximum for station 11), and the temperature

ratio T_w/T_v at each station increased from about 1.2 to approximately 2.0. Over this wide range of conditions, there is fair agreement between laminar theory and the experimental C_H data for each of these three stations, with the largest discrepancies generally occurring at times near 15 seconds when the accuracy of the experimental data is poorest because of the small slopes of the temperature-time curves. (See fig. 4(b).)

At stations 12.5, 14, 15.5, and 17 (figs. 5(d), 5(e), 5(f), and 5(g)), the data were in fair agreement with the laminar theory until $t = 17.0$ seconds. As R_v approached its maximum value, which occurred at 17.4 seconds, the C_H values at each of these four stations increased towards turbulent magnitude, and later, during the period of decreasing R_v, returned to laminar magnitude. The highest values of C_H at station 12.5 were transitional (halfway between laminar and turbulent), whereas at stations 14, 15.5, and 17, they were in agreement with turbulent theory based on length from the nose tip, although turbulent flow obviously did not start at the nose tip. The rise in C_H apparently began simultaneously at these four stations and therefore at different values of R_v at each station. At 17.0 seconds, values of R_v were 18.5×10^6 and 25.2×10^6 at stations 12.5 and 17, respectively. However, the more rearward stations (of this group of four) remained turbulent longer, so that the values of R_v when C_H again became laminar were approximately the same at each station $\left(19.2 \times 10^6, 18.6 \times 10^6, 18.8 \times 10^6,\right.$ and $\left.20.6 \times 10^6\right.$ at stations 12.5, 14, 15.5, and 17, respectively$\left.\right)$. During the remainder of the test, R_v remained less than these values, and C_H at stations 12.5 and 14 were continuously in agreement with laminar theory, whereas at stations 15.5 and 17, the data tended to be somewhat above laminar theory.

The data for the two most rearward measurement points, stations 25 and 29, are shown in figures 5(h) and 5(i). The heat-transfer coefficients were laminar at station 25 until the interval between 16.5 and 16.75 seconds when the rise toward turbulent magnitude began at this station. The value of R_v was 33×10^6 at 16.75 seconds. Although transitional flow began apparently simultaneously at the four previous stations, the fact that it began 0.25 second earlier at this station discounts the possibility that a disturbance, such as angle of attack, initiated transition all along the nose. After C_H rose to turbulent magnitude at station 25, it was in fair agreement with turbulent theory based on length from the nose tip during the remainder of the test, except for transitional values near 20.5 seconds when R_v decreased to its mimimum value of 24.5×10^6. This minimum was not as low as the R_v values of about 20×10^6 at which the four previous stations became laminar.

At station 29, C_H was turbulent or transitional even during the early part of the test period. Although station 25 was laminar at values of R_V as high as 30×10^6 (t = 16.5 seconds), station 29 was transitional at $R_V = 22 \times 10^6$ (t = 15.5 seconds). After the time of maximum R_V, C_H for this station was consistently in good agreement with the turbulent theory based on length from the nose tip, with no indication of transitional flow as R_V decreased to the minimum of 28.5×10^6.

According to the theory of reference 12, skin friction and heat transfer on cones in supersonic flow are functions only of the local flow conditions, and independent of cone angle as such. Therefore, the heat-transfer data obtained in the present 15° nose cone can be compared directly with measurements on the 10° cones of references 1, 2, and 5 at similar local-flow conditions. Data from these references are plotted on figures 5(e), 5(h), and 5(i) for comparison with the present measurements, and table I lists the local conditions for the reference data and for the present test.

In figure 5(e), it is interesting to note that the data of reference 5 show laminar heat transfer changing to turbulent magnitude and then back to laminar as did the present data during this particular variation of local conditions. The laminar measurement from reference 5 plotted at 16.5 seconds is in good agreement with the present data. In figure 5(h) it is seen that the present data are laminar or transitional at some conditions for which data of reference 5 were turbulent; however, when the present data were turbulent, they were in good agreement with the data of reference 5. Figure 5(i) shows that the turbulent data of references 1 and 2 are in good agreement with the present measurements at similar local flow conditions.

TRANSITION

The location of transition and the comparison of the experimental data with laminar and turbulent theory along the nose at particular times are best seen in the plots of figure 6, which show C_H against length along the cone at each time for which data were reduced. It is apparent from these plots that the loss of data from station 21, while unfortunate, is really significant at only a few times, such as 19.0 seconds when the transition from laminar to turbulent flow took place between stations 17 and 25.

From figure 6, it can be seen that over the complete range of the test, the laminar theory closely predicted the level and trend with nose length of the laminar C_H data, which at times extended as far back as

station 25 (that is, times 15.5 seconds to 16.5 seconds). Surprisingly, the turbulent theory, based on length from the nose tip, predicted almost equally well the level and trend with nose length (that is, Reynolds number) of the fully turbulent C_H data.

It would be expected that the turbulent theory based on length from the nose tip would underestimate turbulent C_H behind a transition occurring at a reasonably large Reynolds number, as in the present test, since length from the nose tip would be much more than the effective turbulent length, that is, the length required to develop the existing momentum thickness assuming turbulent growth rate. For instance, the effective turbulent length at 18.0 seconds was computed to be 0.67 inch, using the assumption that Van Driest's cone theory (ref. 12) is valid for turbulent flow on a frustum of a cone. Thus, the effective origin of the turbulent boundary layer was at station 13.33 or 0.67 inch ahead of the transition station (station 14). The Van Driest turbulent theory for cones based on length from this origin is plotted for time 18.0 seconds in figure 6(d). The theory based on length from the beginning of transition (station 14) is also shown for comparison. It is obvious that either of these methods would have overpredicted almost all, if not all, of the turbulent C_H data obtained in this test.

It is interesting to note that at the earlier times (15 to 17 seconds) the skin temperatures were approximately the same at all stations except the rearmost, whereas after 17.75 seconds gradients as large as 100° F per inch existed along the skin. (See fig. 4(b).) Nevertheless, no significant variation is apparent in the C_H distributions of figure 6 which might be attributed to the influence of surface temperature distribution, and the theories, which assume isothermal surface conditions, agree equally well with the measurements at times of large and small gradients.

Figure 6 shows that there was considerable variation in the extent of transitional flow along the nose, both in Reynolds number and in distance. For instance, at 17 seconds, the flow was transitional for at least 12 inches (station 17 to station 29), equivalent to a Reynolds number span of 17.9×10^6; whereas at 17.5 seconds the flow was transitional only between stations 11 and 14, a distance of 3 inches and equivalent to a Reynolds number span of 4.82×10^6. The variation in extent of transitional flow does not seem to correlate with any of the basic variables such as Mach number, R_V/ft, or transition Reynolds number.

Values of transition Reynolds number R_{tr}, defined herein as local Reynolds number at the beginning of transition from laminar to turbulent flow, were determined from the C_H distributions of figure 6 and are noted thereon. The beginning of transition was assumed to occur at the

most rearward measurement station having a laminar C_H value. Although laminar C_H may exist somewhat downstream of the last laminar measurement station, the station spacing is such that with one exception R_{tr} determined in this manner could be no more than about 10 percent too small. The exception is when station 17 was the most rearward laminar station, in which case R_{tr} could be as much as 35 percent greater than the value based on station 17 (because of the loss of data from station 21). In figure 6, R_{tr} is noted on the basis of the last laminar station, but in subsequent figures where values of R_{tr} are plotted, the probable range of R_{tr} is indicated for the cases where station 17 was the most rearward laminar station. Because determination of the beginning of transition at 21.5 and 22.0 seconds would be very arbitrary, no values of R_{tr} have been specified for these times.

In figure 7, the temperature ratio T_w/T_v at the transition station is plotted against local Mach number. During the large increase in Mach number from 1.42 to 3.84, T_w/T_v remained about constant at 1.2; and during the increase in Mach number from 3.33 to 4.64, T_w/T_v was approximately constant near 2.4. During the coast period, T_w/T_v rose from 1.23 to 2.27 whereas the decrease in Mach number was relatively small (from 3.84 to 3.33). This pattern makes it possible to plot the variation of R_{tr} with M_v at nearly constant T_w/T_v, and its variation with T_w/T_v at approximately constant M_v, as is done in subsequent figures.

The values of R_{tr} corresponding to each point are noted in the figure. The largest value of R_{tr} was 30.3×10^6 and occurred at 16.5 seconds when M_v and T_w/T_v were 2.91 and 1.15, respectively. The lowest value of R_{tr} was 14.2×10^6 and occurred at 15.0 seconds when M_v and T_w/T_v were 1.41 and 1.15, respectively.

The broken curve in figure 7 shows the variation of the ratio T_{aw}/T_v for a recovery factor of 0.88. While it might be expected that R_{tr} would be greater when T_w was colder with respect to T_{aw}, this trend is not substantiated by the data.

Conditions of M_v and T_w/T_v below the solid line are those for theoretically infinite stability of the laminar boundary layer for two-dimensional disturbances, as given by reference 15. As the Mach number increased from 1.42 to 2.91 and the test conditions progressed into this stability region, R_{tr} increased considerably; but this trend reversed as the test conditions went farther into the region. As stated previously,

the plotted values of T_w/T_v are those at the transition stations; but at more forward stations, T_w/T_v generally had a lower value. For instance, at time 22.5 seconds ($M = 4.23$, $R_{tr} = 17.1 \times 10^6$) T_w/T_v was 2.4 at the transition point, station 15.5, but was less than 2.0 at all measurement points from station 12.5 forward. The value $T_w/T_v = 2.4$ is considerably outside the two-dimensional stability region at M_v of 4.23, whereas the values of less than 2.0 are within it. The influence on R_{tr} of such variations of T_w/T_v along the surface is not known.

An extension of the two-dimensional stability theory, made by Dunn and Lin (ref. 16), indicates that infinite stability to three-dimensional disturbances does not exist at any condition of M_v and T_w/T_v, although stability to very large Reynolds numbers ($\sim 10^{12}$) might be obtained at somewhat colder wall conditions than those for infinite stability to two-dimensional disturbances. The temperature-ratio condition was computed in reference 16 to be 1.474 for Mach number 4. Although a condition of $T_w/T_v = 1.23$ at $M_v = 3.84$ was obtained during the present test, the corresponding value of R_{tr} was only 17.7×10^6.

Figure 8(a) shows the variation of the experimental values of R_{tr} with M_v during the two periods of approximately constant T_w/T_v noted in figure 7. The open symbols are for a temperature ratio near 1.2, whereas the solid symbols are for a temperature ratio of approximately 2.4. The time to which the data correspond and the transition station and its temperature ratio are noted in the key. As noted previously, the values of R_{tr} may be too small in cases where station 17 was chosen as the transition location. For these cases the probable range of R_{tr} is indicated. Also, at times 15.0 and 17.0 seconds, there is some doubt in the selection of the transition station (see figs. 6(a) and 6(c)), and R_{tr} is plotted as a range for these times also. The data for T_w/T_v near 1.2 show that R_{tr} doubled as M_v increased from 1.42 to 2.91, and then decreased by half as M increased to 3.75. As M_v further increased to 3.84, R_{tr} was constant. It should be noted that these variations in R_{tr} are not due exclusively to M_v; for although T_w/T_v was essentially constant, the wall temperature became colder with respect to T_{aw} as M_v increased. (See fig. 7.)

For a temperature ratio near 2.4, the value of R_{tr} is essentially constant from Mach number 3.61 to Mach number 4.64 and is close to that for a temperature ratio of 1.2.

Transition Reynolds numbers reported in reference 5 for a 10° total angle cone are also shown in figure 8(a). The temperature ratios for

these data were from 1.19 to 1.36. The values of R_{tr} were about 50 percent of the present values at Mach numbers below 3; however, as in the present test, R_{tr} increased with Mach number up to a value of Mach number at which R_{tr} decreased sharply. The decrease occurred between Mach numbers 3 and 3.5 in the present test and near 3.5 in the test of reference 5.

The values of R_{tr} obtained during the coasting period, while T_w/T_v was increasing and Mach number was approximately constant, are shown in figure 8(b). The Mach number actually varied from 3.84 to 3.33 as shown in the key, but this variation is less than ±8 percent from an average of 3.55. The values of R_{tr} are plotted against the wall-temperature parameter $\left(T_w - T_{aw}\right)/T_{so}$, which indicates the aerodynamic heating condition more clearly than the ratio T_w/T_v. At values of $\left(T_w - T_{aw}\right)/T_{so}$ from -0.15 to -0.23, the influence of the temperature parameter on R_{tr} is obscured by the range of uncertainty of the measured R_{tr}. However, it appears probable that R_{tr} increased slightly as the temperature parameter became more negative in this range. At values of $\left(T_w - T_{aw}\right)/T_{so}$ from -0.34 to -0.55 R_{tr} seems independent of the temperature parameter. Also shown in figure 8(b) are flight measurements of R_{tr} at Mach numbers near 3.7 on the 10° total angle cone of reference 5. While these values of R_{tr} are lower than in the present case, the trends with wall-temperature parameter appear to be somewhat similar in the two groups of data.

COMPUTED SKIN TEMPERATURES

In order to determine the accuracy with which the experimental skin temperatures could be predicted, computations of skin temperature at station 11 and at station 29 were made for the flight conditions by using theoretical laminar and turbulent heat-transfer coefficients, respectively, and by assuming an emissivity of 0.3. The resultant temperature time histories are shown in figure 9 along with the measured temperatures. The laminar theory predicted the measured temperature at station 11 with a maximum discrepancy of about 40°, and the turbulent theory based on length from the nose tip did likewise for the measured temperature at station 29.

CONCLUDING REMARKS

Measurements of aerodynamic heat transfer have been made at nine stations on the 31-inch long 15° total angle conical nose of a rocket-propelled model at Mach numbers up to 5.2. The maximum local Mach number just outside the boundary layer on the cone was 4.65. Local Reynolds numbers based on length from the nose tip to a measurement station covered the range from 3.8×10^6 to 46.5×10^6.

Laminar, transitional, and turbulent heat-transfer coefficients were measured. The laminar data agreed well with flat-plate laminar theory increased by $\sqrt{3}$ to account for the conical nose shape. The turbulent data agreed well with turbulent theory for skin friction on cones using Reynolds number based on length from the nose tip, and the modified Reynolds analogy (Stanton number equals 0.6 of the local skin friction coefficient).

Reynolds numbers at the beginning of transition, determined from the heat-transfer coefficients, varied from 14.2×10^6 to 30.3×10^6. Considerable variation was noted in the length of the transitional region.

At a relatively constant ratio of wall to static temperature of 1.2, the transition Reynolds number doubled as Mach number increased from 1.42 to 2.91 and then decreased by half as Mach number increased from 2.91 to 3.75. As Mach number continued to increase to 3.84, the transition Reynolds number was constant.

At ratios of wall to static temperature near 2.4, the transition Reynolds number was essentially constant at Mach numbers from 3.61 to 4.64, and was close to the value for a temperature ratio of 1.2.

At Mach numbers near 3.5, the transition Reynolds number seemed independent of the skin-temperature parameter, wall temperature minus adiabatic wall temperature divided by stagnation temperature, at values of the temperature parameter from -0.34 to -0.55.

The transition Reynolds number was 17.7×10^6 at a condition of Mach number and ratio of wall to static temperature near that for which three-dimensional disturbance theory has been evaluated and has predicted laminar boundary-layer stability to very high Reynolds numbers $\left(\sim 10^{12}\right)$.

Langley Aeronautical Laboratory,
National Advisory Committee for Aeronautics,
Langley Field, Va., June 12, 1956.

REFERENCES

1. Rumsey, Charles B., Piland, Robert O., and Hopko, Russell N.: Aerodynamic-Heating Data Obtained From Free-Flight Tests Between Mach Numbers of 1 and 5. NACA RM L55A14a, 1955.

2. Rumsey, Charles B.: Free-Flight Measurements of Aerodynamic Heat Transfer to Mach Number 3.9 and of Drag to Mach Number 6.9 of a Fin-Stabilized Cone-Cylinder Configuration. NACA RM L55G28a, 1955.

3. Piland, Robert O., and Collie, Katherine A.: Aerodynamic Heating of Rocket-Powered Research Vehicles at Hypersonic Speeds. NACA RM L55E10c, 1955.

4. Piland, Robert O., Collie, Katherine A., and Stoney, William E.: Turbulent and Laminar Heat-Transfer Measurements on a 1/6-Scale NACA RM-10 Missile in Free Flight to a Mach Number of 4.2 and to a Wall Temperature of 1400° R. NACA RM L56C05, 1956.

5. Rumsey, Charles B., and Lee, Dorothy B.: Measurements of Aerodynamic Heat Transfer and Boundary-Layer Transition on a 10° Cone in Free Flight at Supersonic Mach Numbers up to 5.9. NACA RM L56B07, 1956.

6. Ginnings, Defoe C., and Thomas, Eugenia: The Electrical Resistance and Total Radiant Emittance of Inconel in the Range 0° to 1000° C. NBS Rep. 4111 (NACA Contract S54-52), Nat. Bur. Standards, May 1955.

7. Staff of the Computing Section, Center of Analysis (Under Direction of Zdeněk Kopal): Tables of Supersonic Flow Around Cones. Tech. Rep. No. 1, M.I.T., 1947.

8. Keenan, Joseph H., and Kaye, Joseph: Thermodynamic Properties of Air Including Polytropic Functions. John Wiley and Sons, Inc., 1945.

9. Woolley, Harold W.: Thermal Properties of Gases. Table 2.10, Nat. Bur. Standards, July 1949.

10. Van Driest, E. R.: Investigation of Laminar Boundary Layer in Compressible Fluids Using the Crocco Method. NACA TN 2597, Jan. 1952.

11. Van Driest, E. R.: Turbulent Boundary Layer in Compressible Fluids. Jour. Aero. Sci., vol. 18, no. 3, Mar. 1951, pp. 145-160, 216.

12. Van Driest, E. R.: Turbulent Boundary Layer on a Cone in a Supersonic Flow at Zero Angle of Attack. Jour. Aero. Sci., vol. 19, no. 1, Jan. 1952, pp. 55-57, 72.

13. Van Driest, E. R.: The Turbulent Boundary Layer With Variable Prandtl Number. Rep. No. AL-1914, North American Aviation, Inc., Apr. 2, 1954.

14. Rubesin, Morris W.: A Modified Reynolds Analogy for the Compressible Turbulent Boundary Layer on a Flat Plate. NACA TN 2917, 1953.

15. Van Driest, E. R.: Calculation of the Stability of the Laminar Boundary Layer in a Compressible Fluid on a Flat Plate With Heat Transfer. Jour. Aero. Sci., vol. 19, no. 12, Dec. 1952, pp. 801-812.

16. Dunn, D. W., and Lin, C. C.: On the Stability of the Laminar Boundary Layer in a Compressible Fluid. Jour. Aero. Sci., vol. 22, no. 7, July 1955, pp. 455-477.

TABLE I

FLIGHT CONDITIONS OF COMPARATIVE DATA

Station 14 (fig. 5(e))				Data from reference 5 (sta. 14)			
Time, sec	M_V	R_V	T_W/T_V	Time, sec	M_V	R_V	T_W/T_V
16.5	2.91	16.9×10^6	1.16	13.8	2.90	17.0×10^6	1.23
17.1	3.62	21.5	1.21	14.5	3.67	21.0	1.32
17.5	3.84	22.4	1.52	14.8	3.80	21.0	1.45
18.0	3.75	20.6	1.77	15.4	3.78	19.6	1.73
18.2	3.70	19.9	1.80	16.4	3.70	17.5	2.02
19.15	3.50	16.6	1.91	16.8	3.68	16.8	2.08

Station 25 (fig. 5(h))				Data from reference 5 (sta. 24)			
Time, sec	M_V	R_V	T_W/T_V	Time, sec	M_V	R_V	T_W/T_V
16.2	2.54	26.4×10^6	1.15	13.5	2.57	25.5×10^6	1.33
18.5	3.63	33.5	2.15	16.0	3.70	30.8	2.22
21.0	3.61	25.7	2.62	18.0	3.60	24.0	2.65

Station 29 (fig. 5(i))				Data from reference 1			
Time, sec	M_V	R_V	T_W/T_V	Time, sec	M_V	R_V	T_W/T_V
15.7	2.03	24.5×10^6	1.20	2.3	2.05	26.6×10^6	1.10
16.5	2.91	35.2	1.30	3.2	2.82	36.5	1.39
20.85	3.52	29.5	2.65	10.4	3.50	26.2	2.22

Station 29 (fig. 5(i))				Data from reference 2			
Time, sec	M_V	R_V	T_W/T_V	Time, sec	M_V	R_V	T_W/T_V
16.15	2.60	31.3×10^6	1.26	13.4	2.50	31.5×10^6	1.27
17.15	3.63	45.4	1.50	14.7	3.60	45.5	1.63
18.65	3.60	37.7	2.22	16.4	3.60	37.8	2.35

CONFIDENTIAL

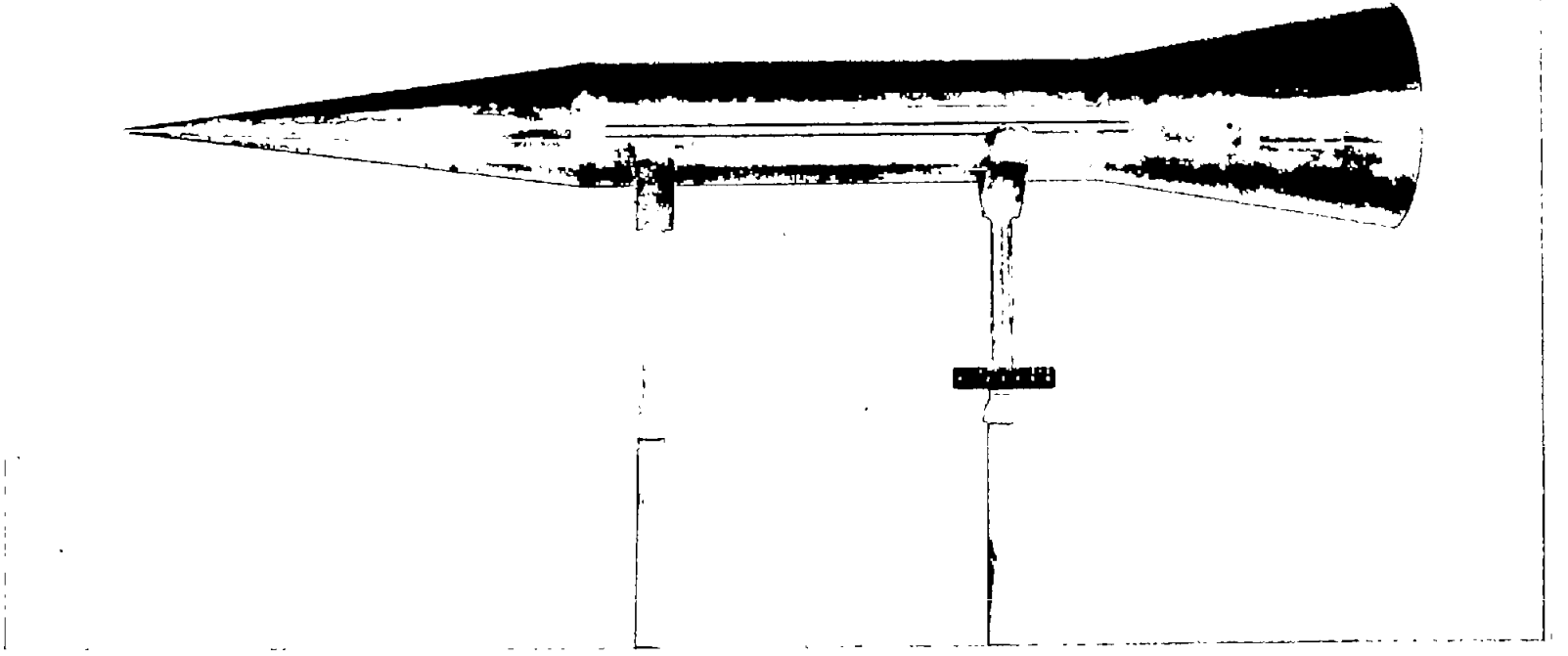

L-86679.1

(a) Photograph of model.

Figure 1.- Test configuration.

CONFIDENTIAL

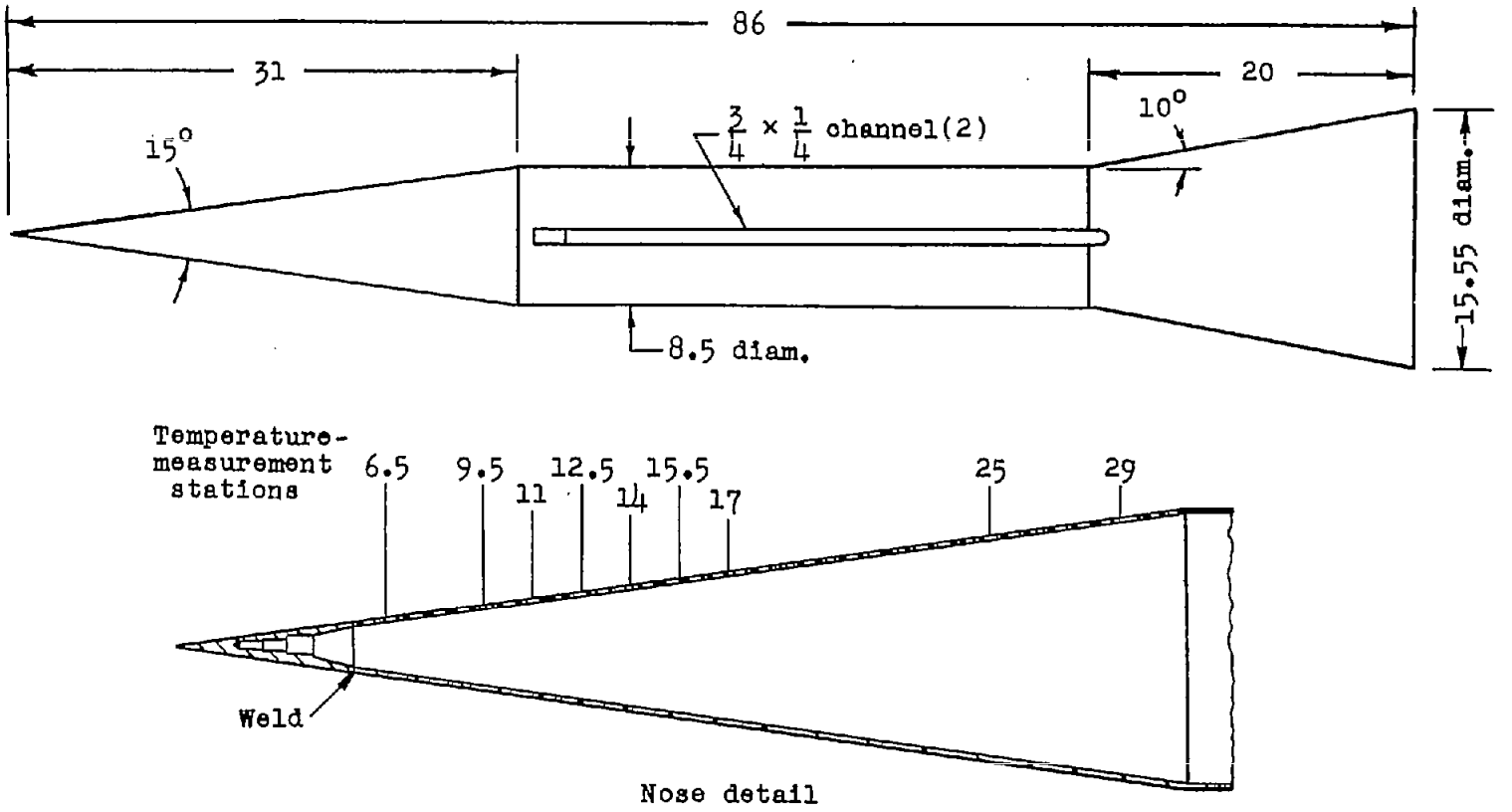

(b) General configuration. Dimensions are in inches.

Figure 1.- Continued.

CONFIDENTIAL

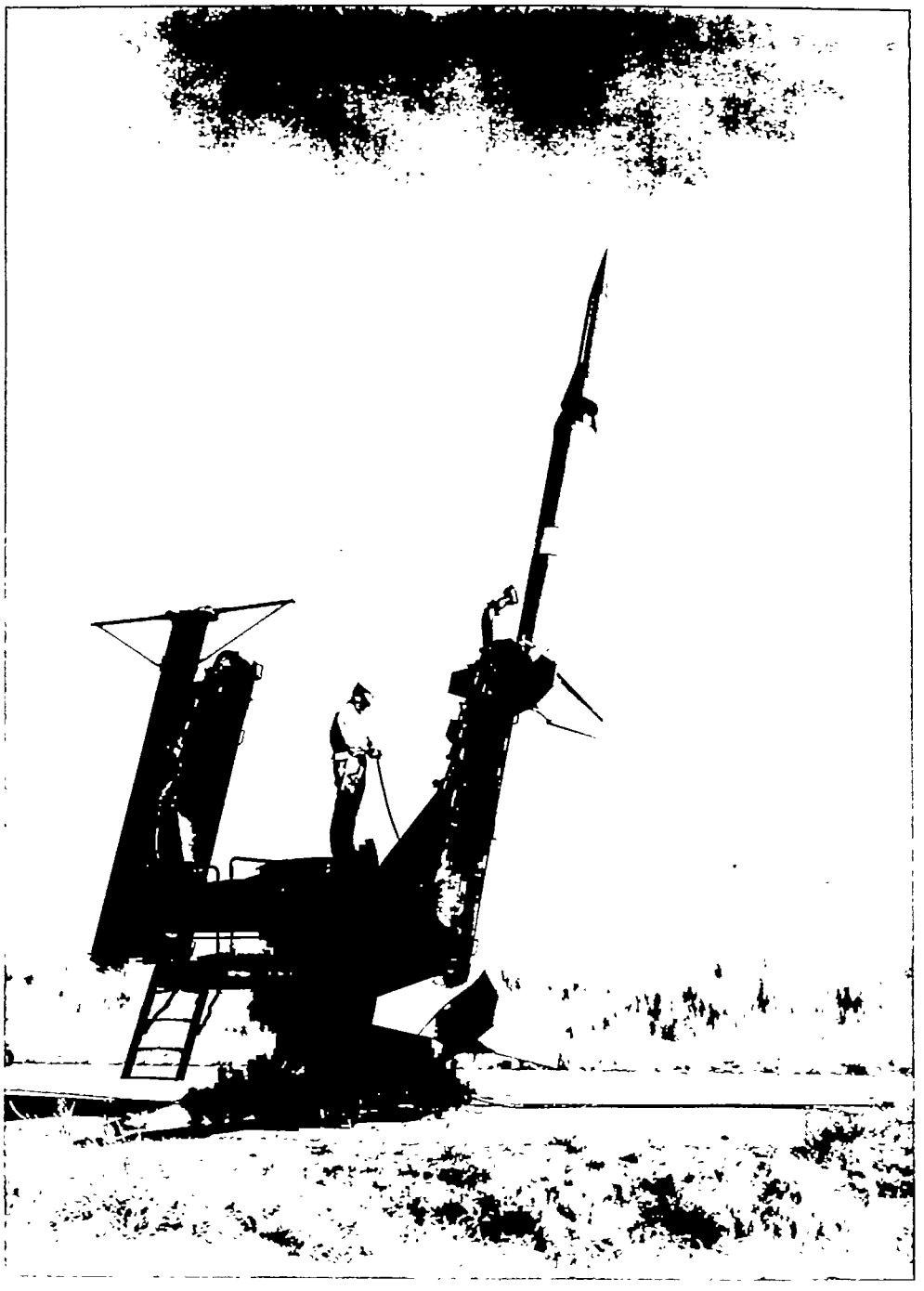

L-87010

(c) Model and boosters on launcher.

Figure 1.- Concluded.

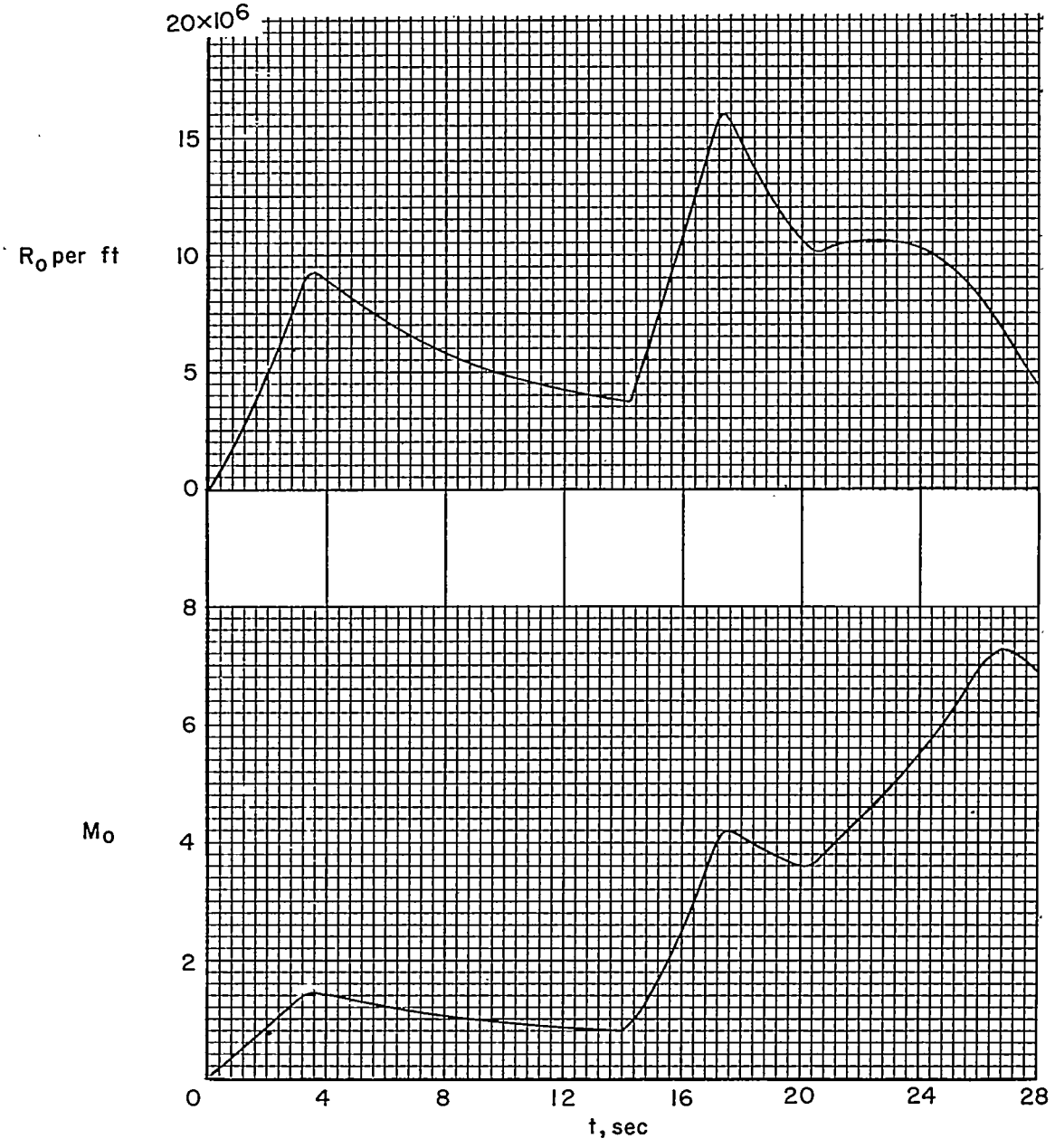

Figure 2.- Test conditions.

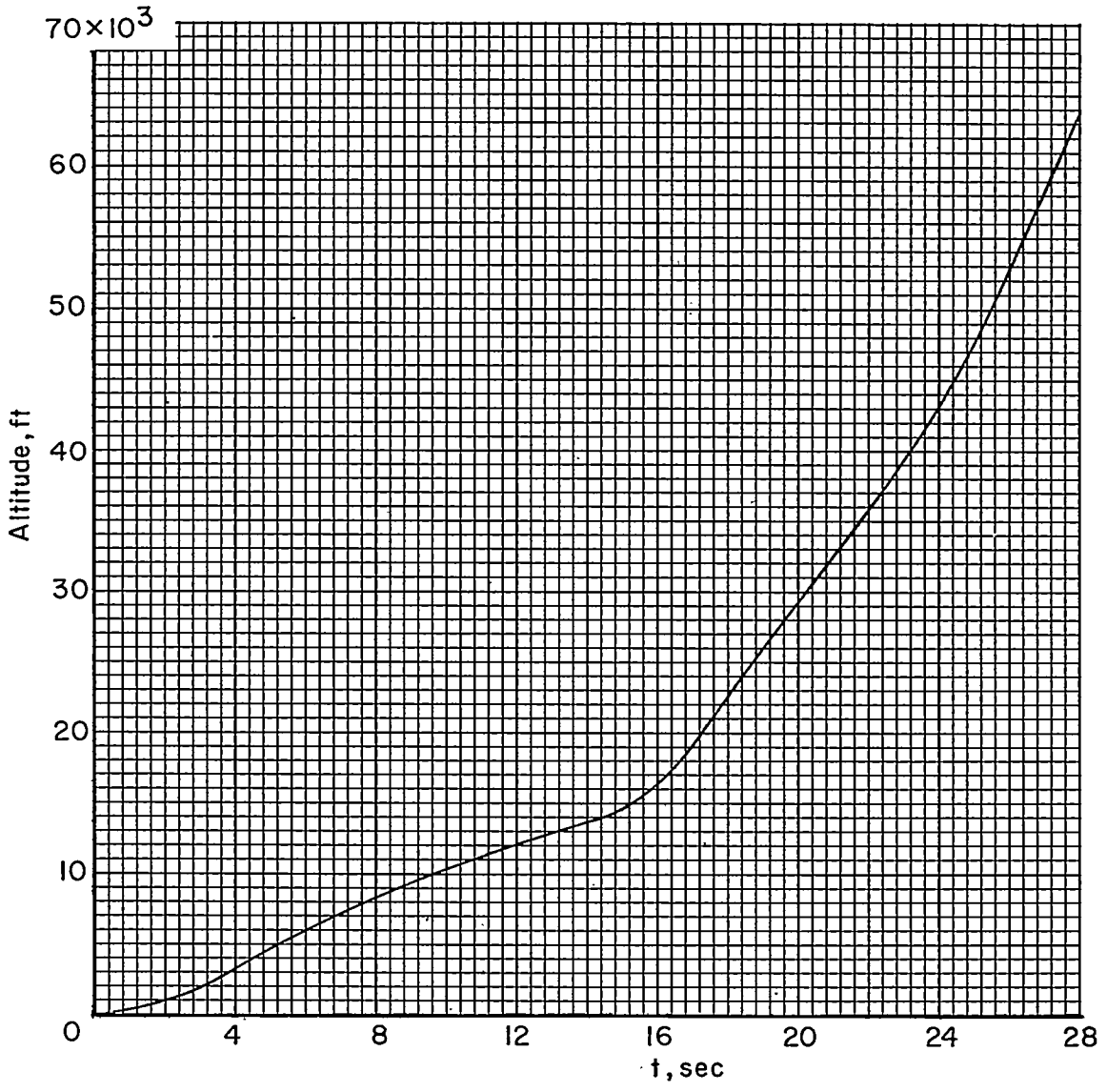

Figure 3.- Altitude time history.

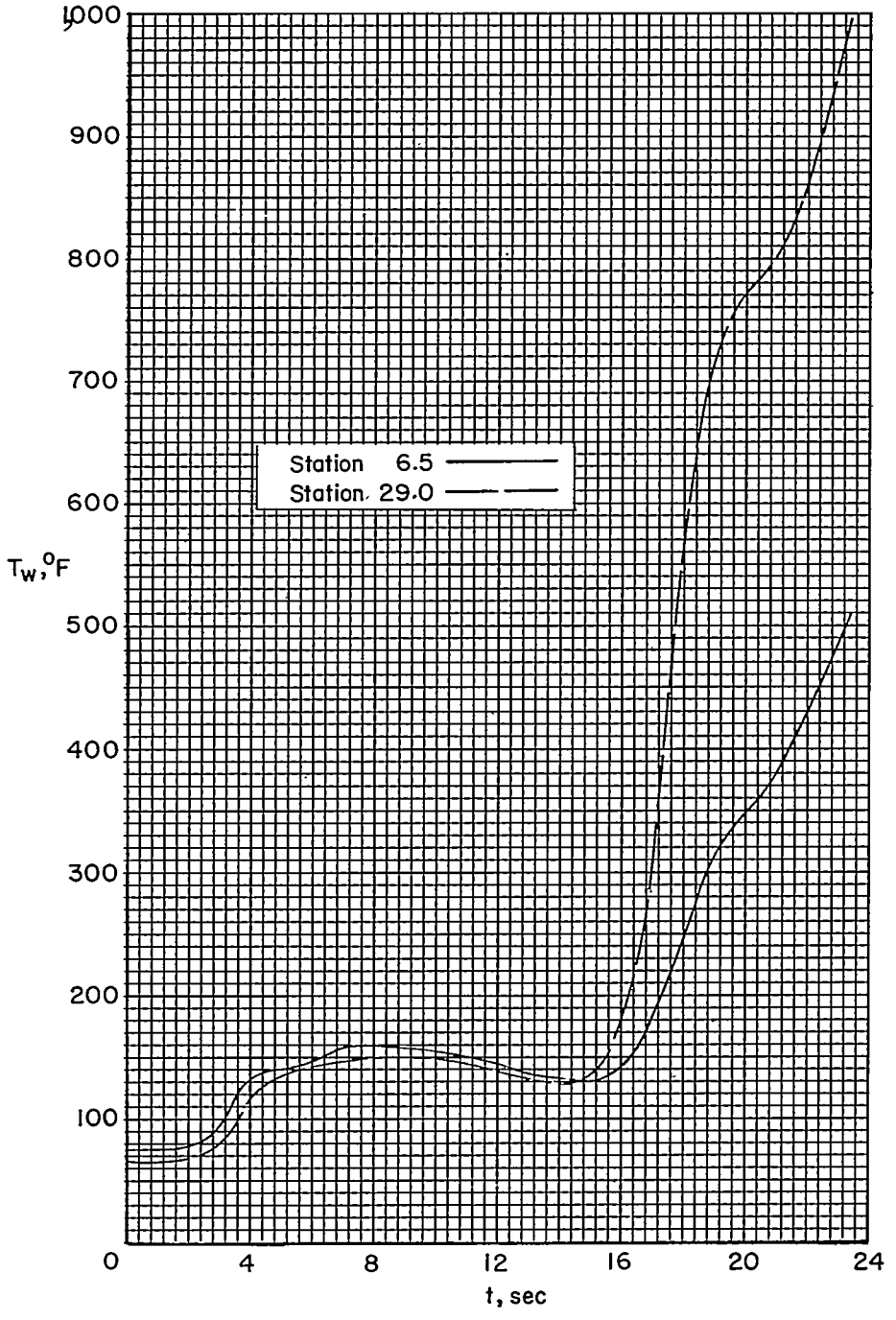

(a) Stations 6.5 and 29.

Figure 4.- Time histories of skin temperatures.

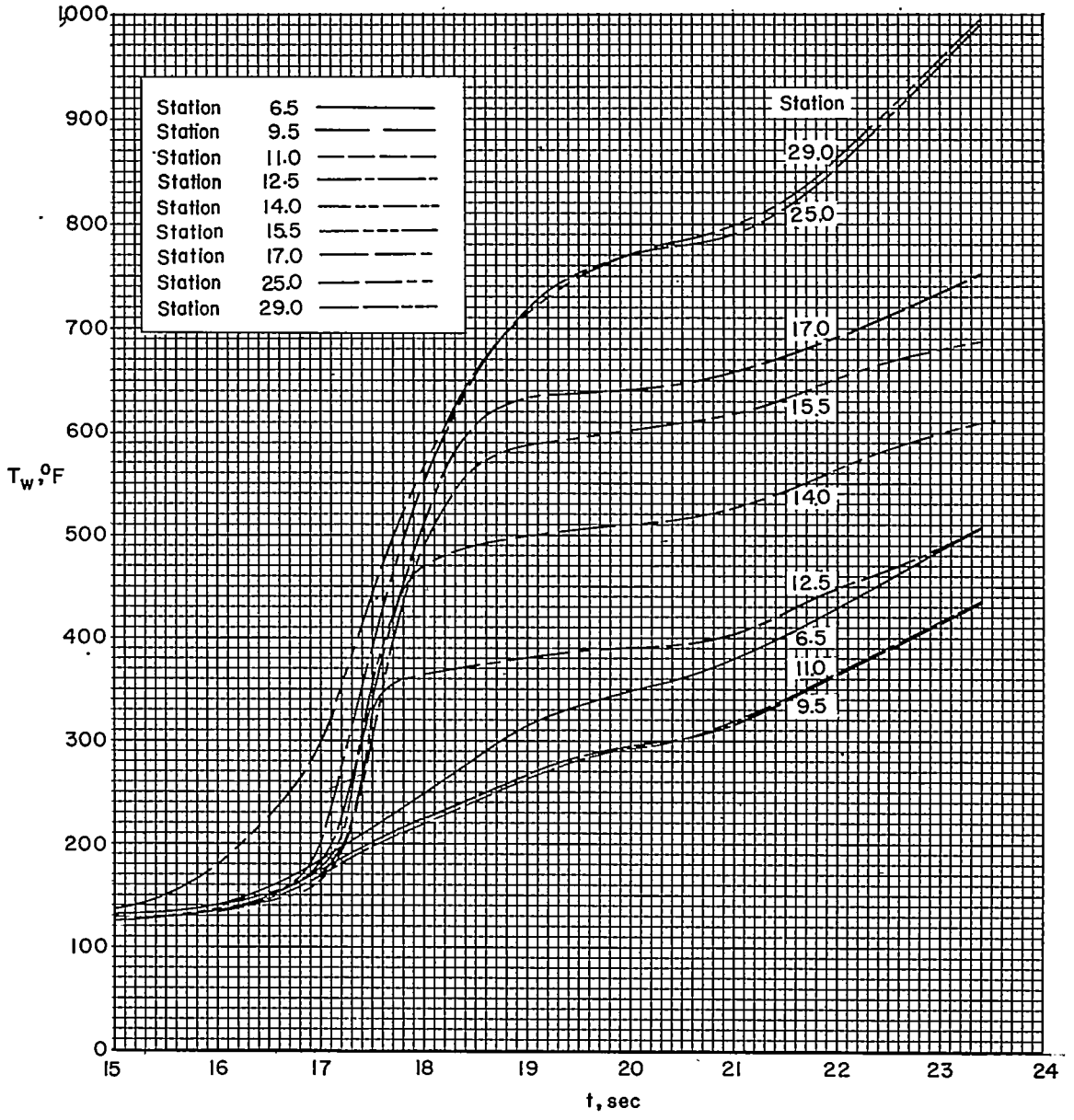

(b) Temperatures after 15.0 seconds.

Figure 4.- Concluded.

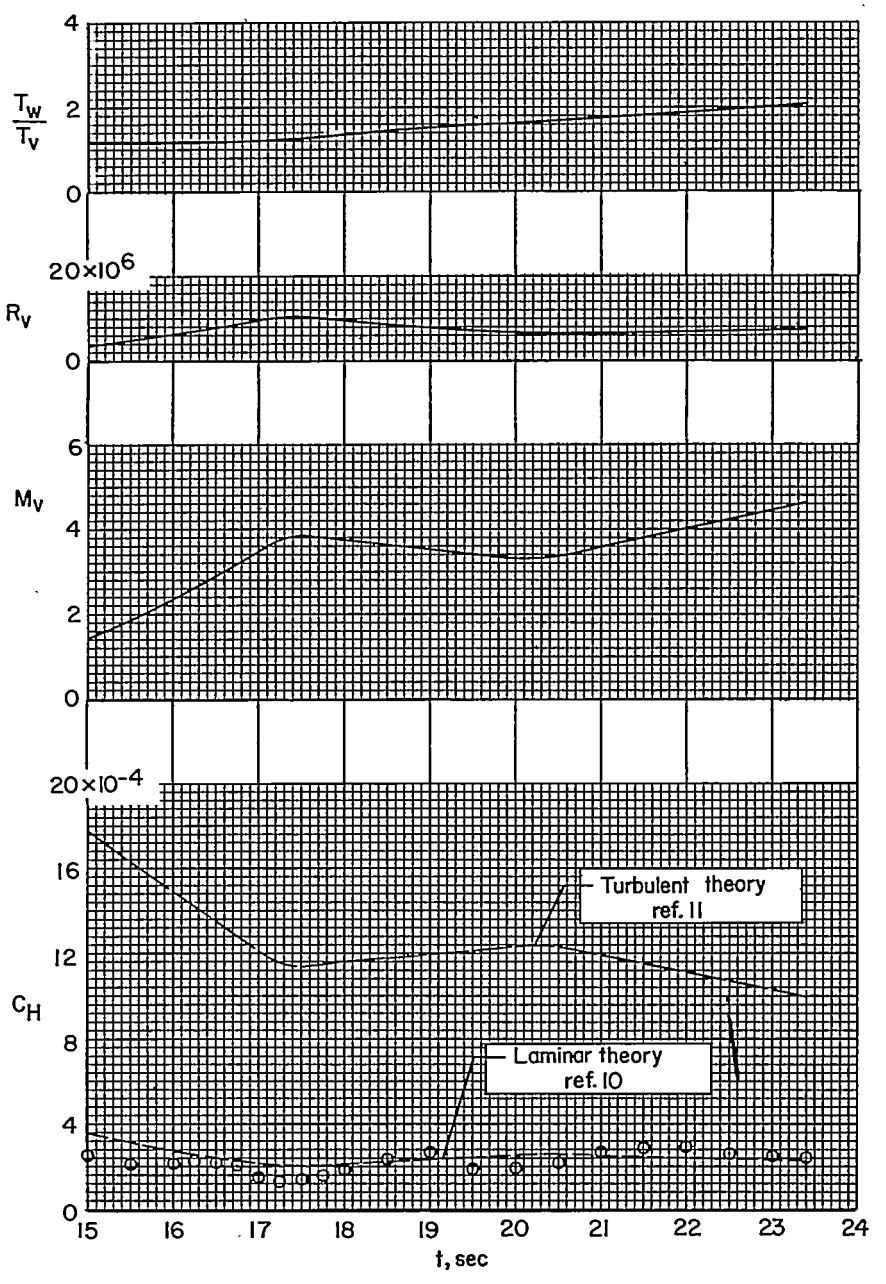

(a) Station 6.5.

Figure 5.- Time histories of C_H at the measurement stations.

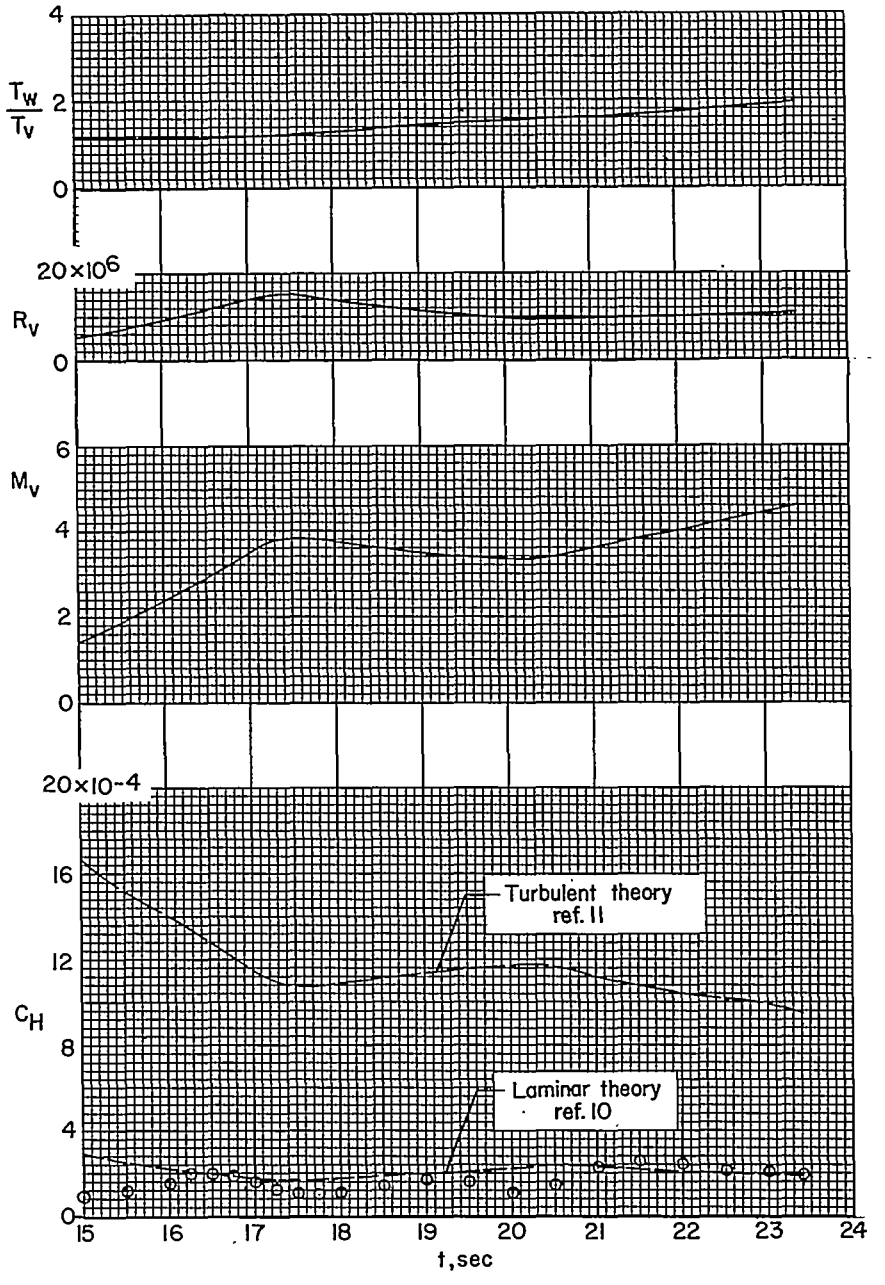

(b) Station 9.5.

Figure 5.- Continued.

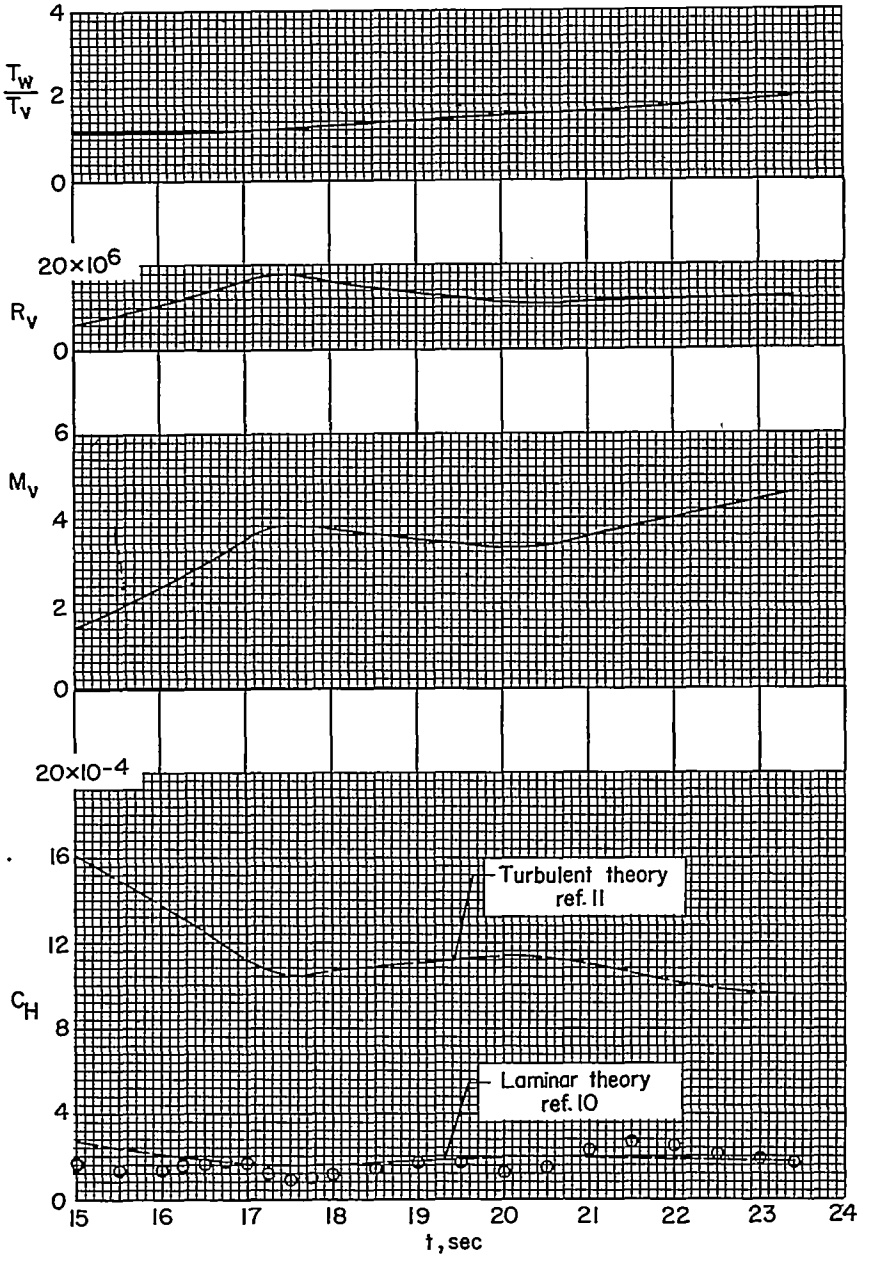

(c) Station 11.

Figure 5.- Continued.

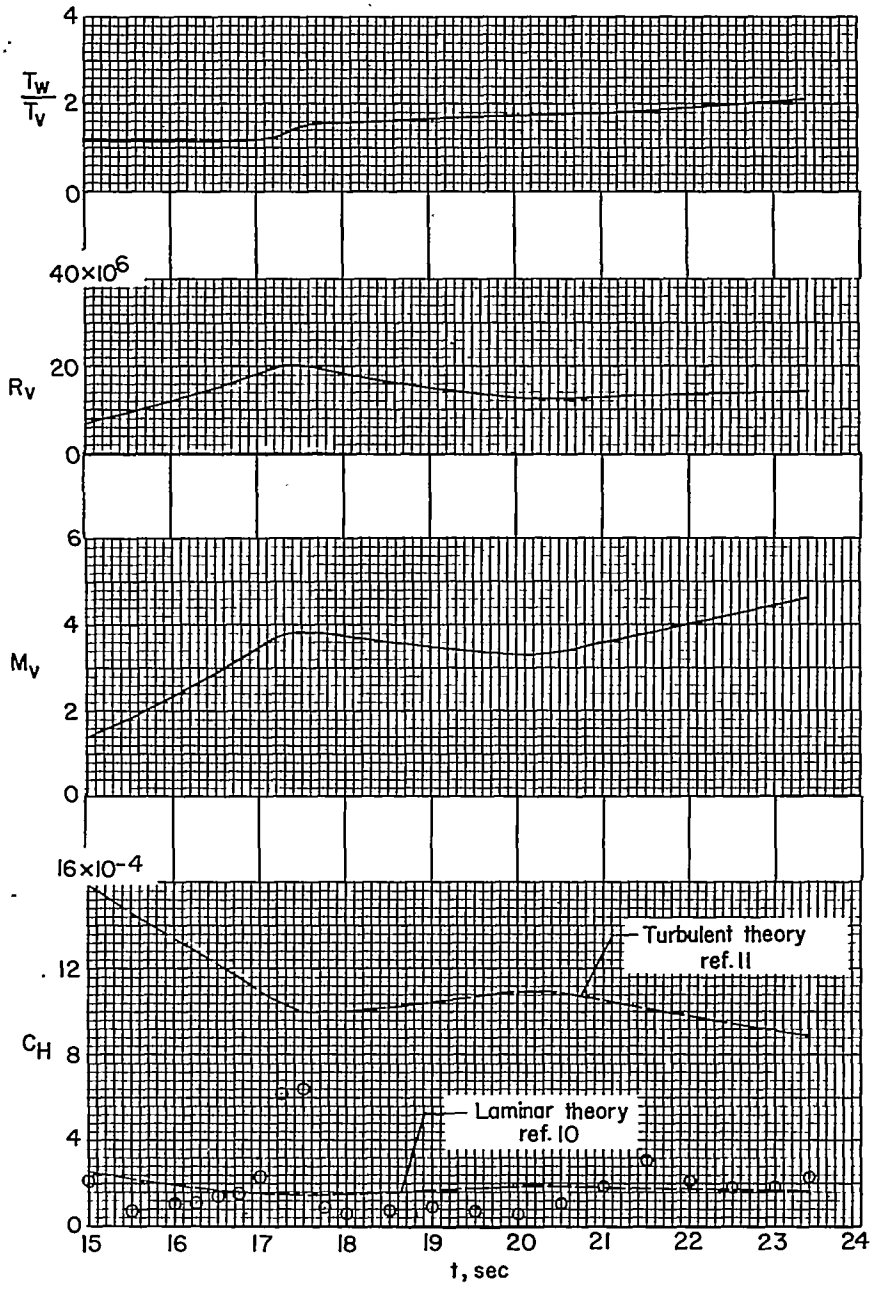

(d) Station 12.5.

Figure 5.- Continued.

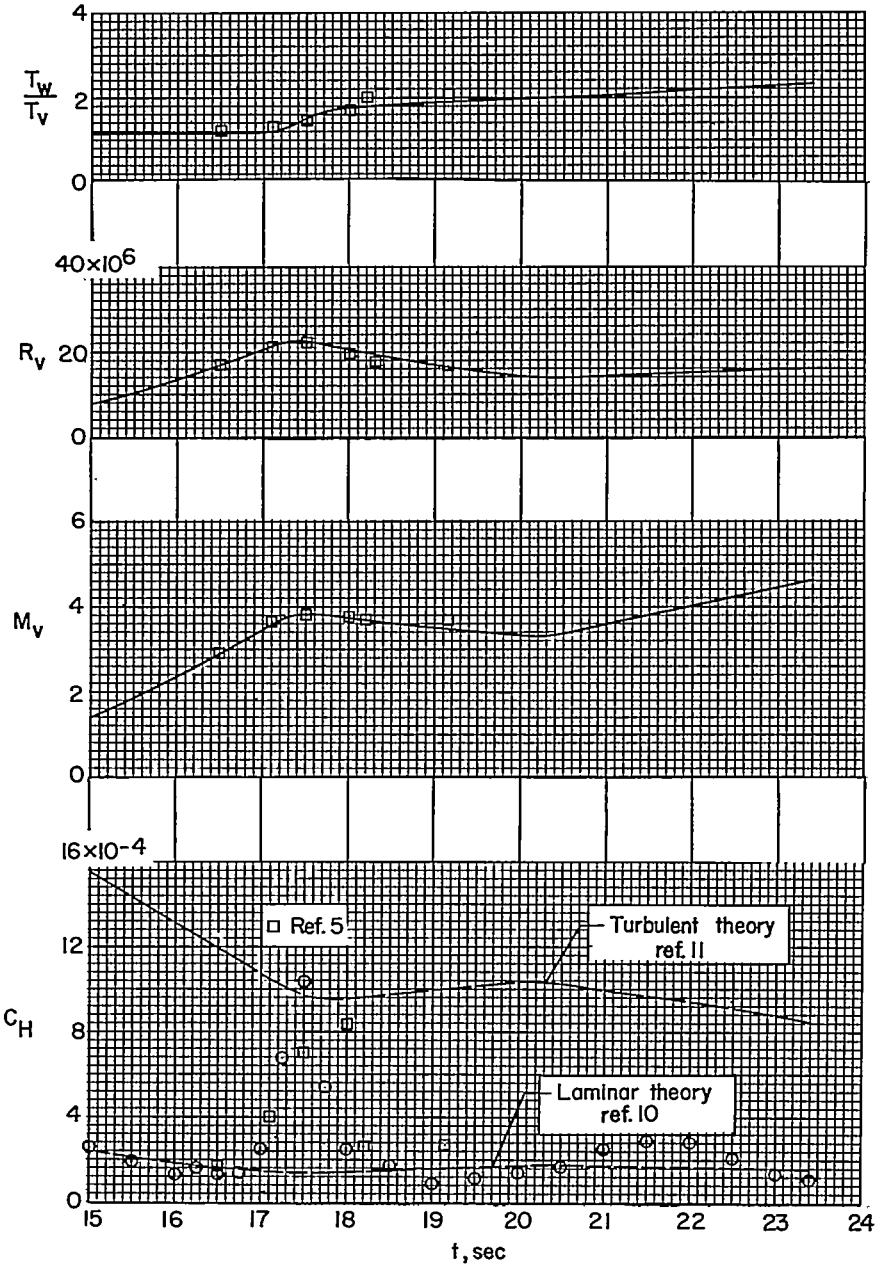

(e) Station 14.

Figure 5.- Continued.

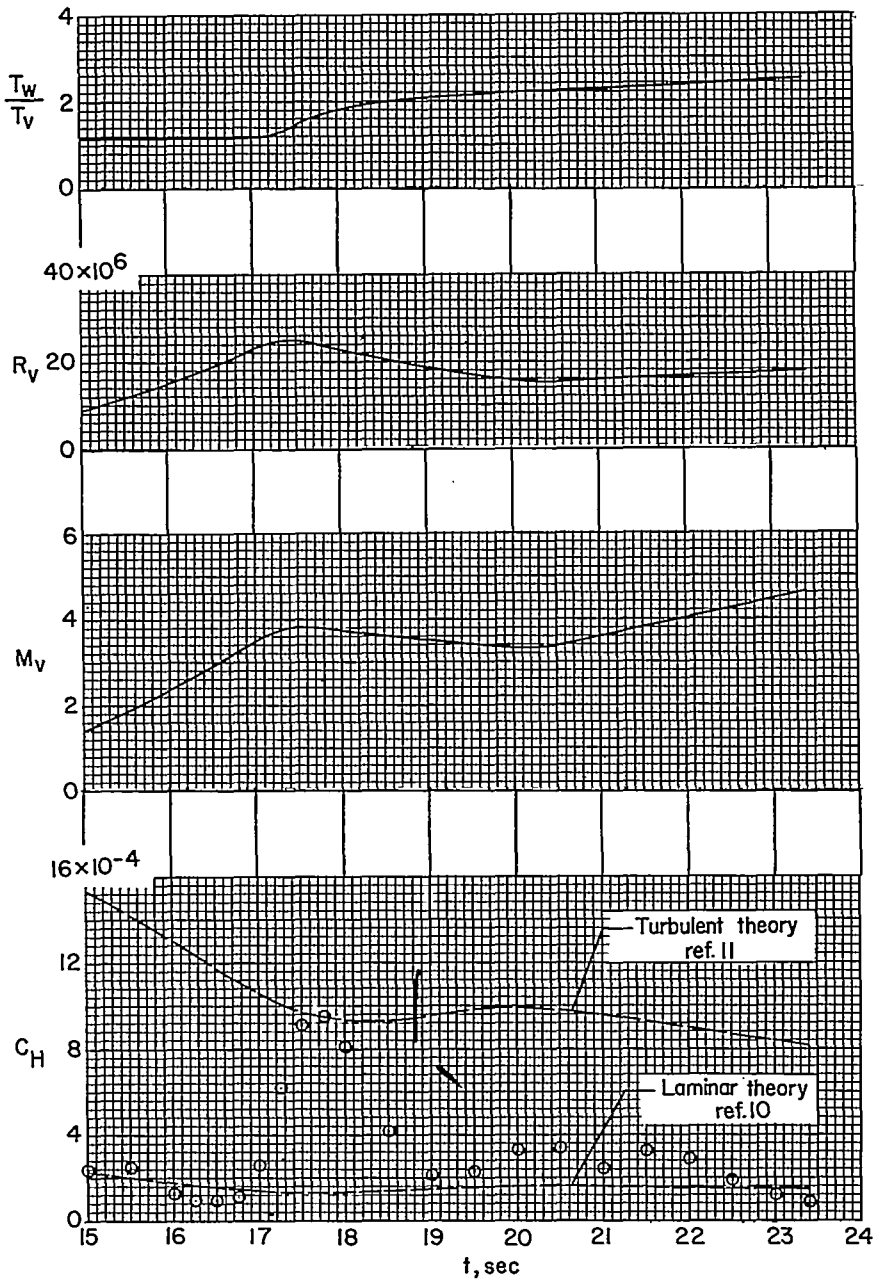

(f) Station 15.5.

Figure 5.- Continued.

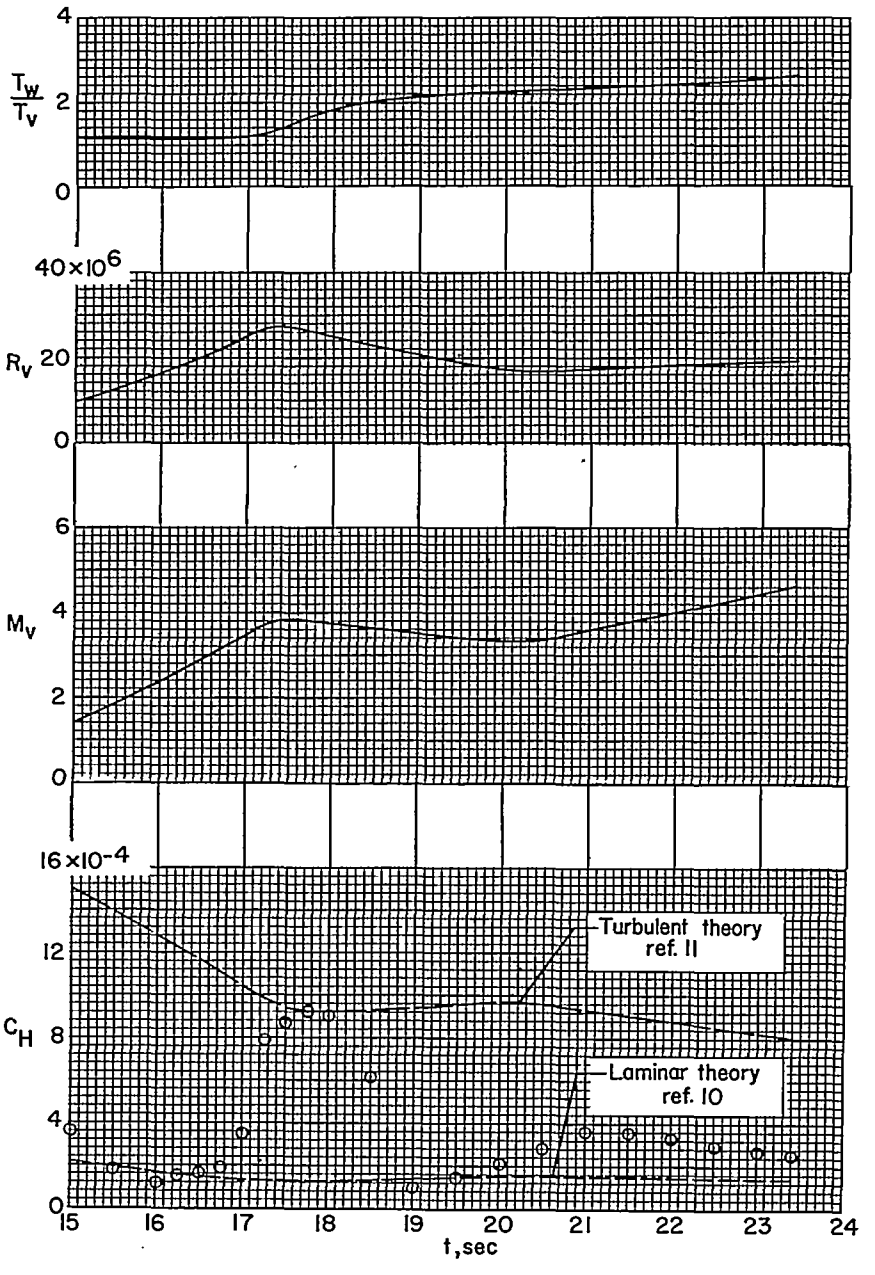

(g) Station 17.

Figure 5.- Continued.

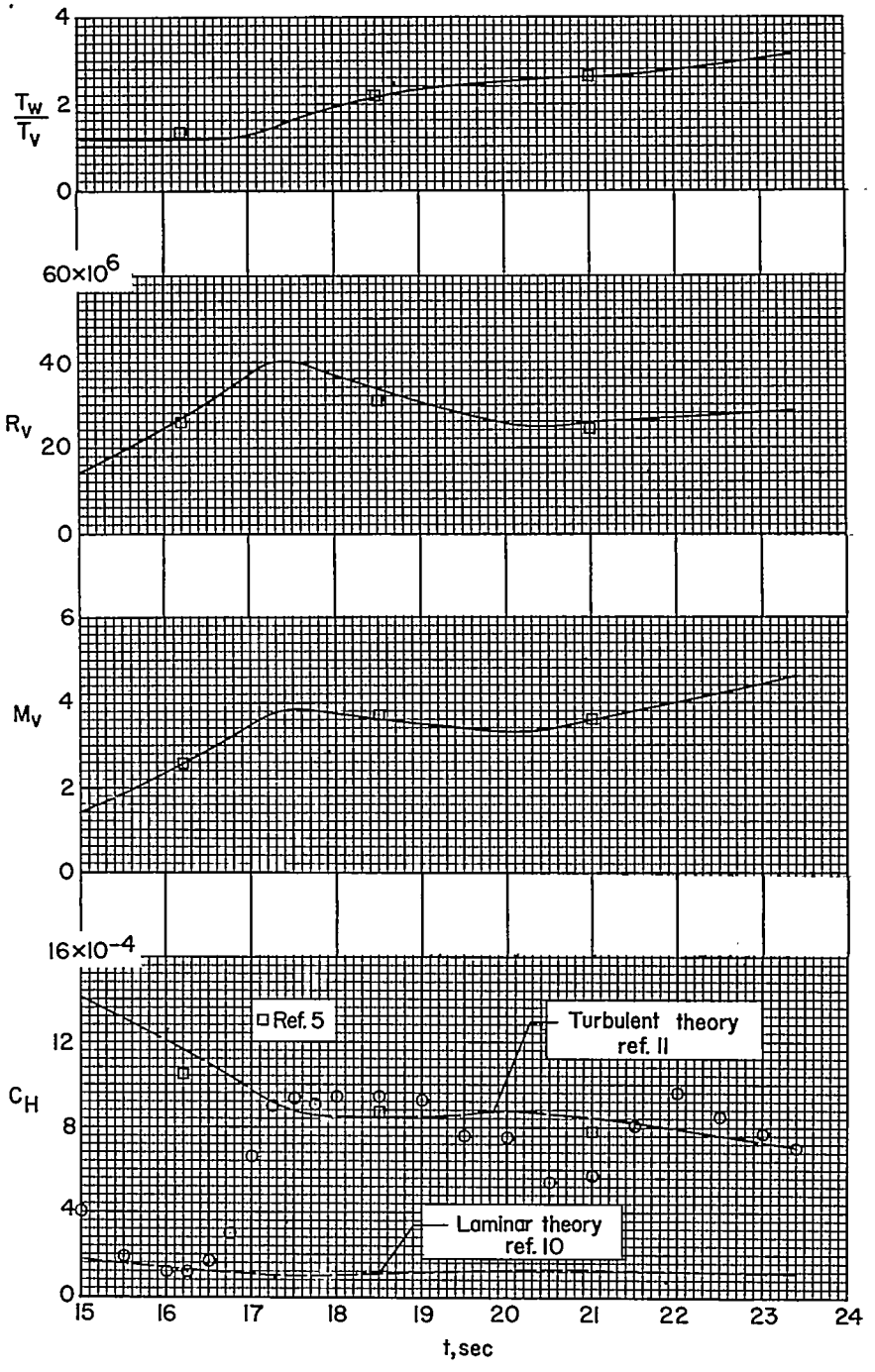

(h) Station 25.

Figure 5.- Continued.

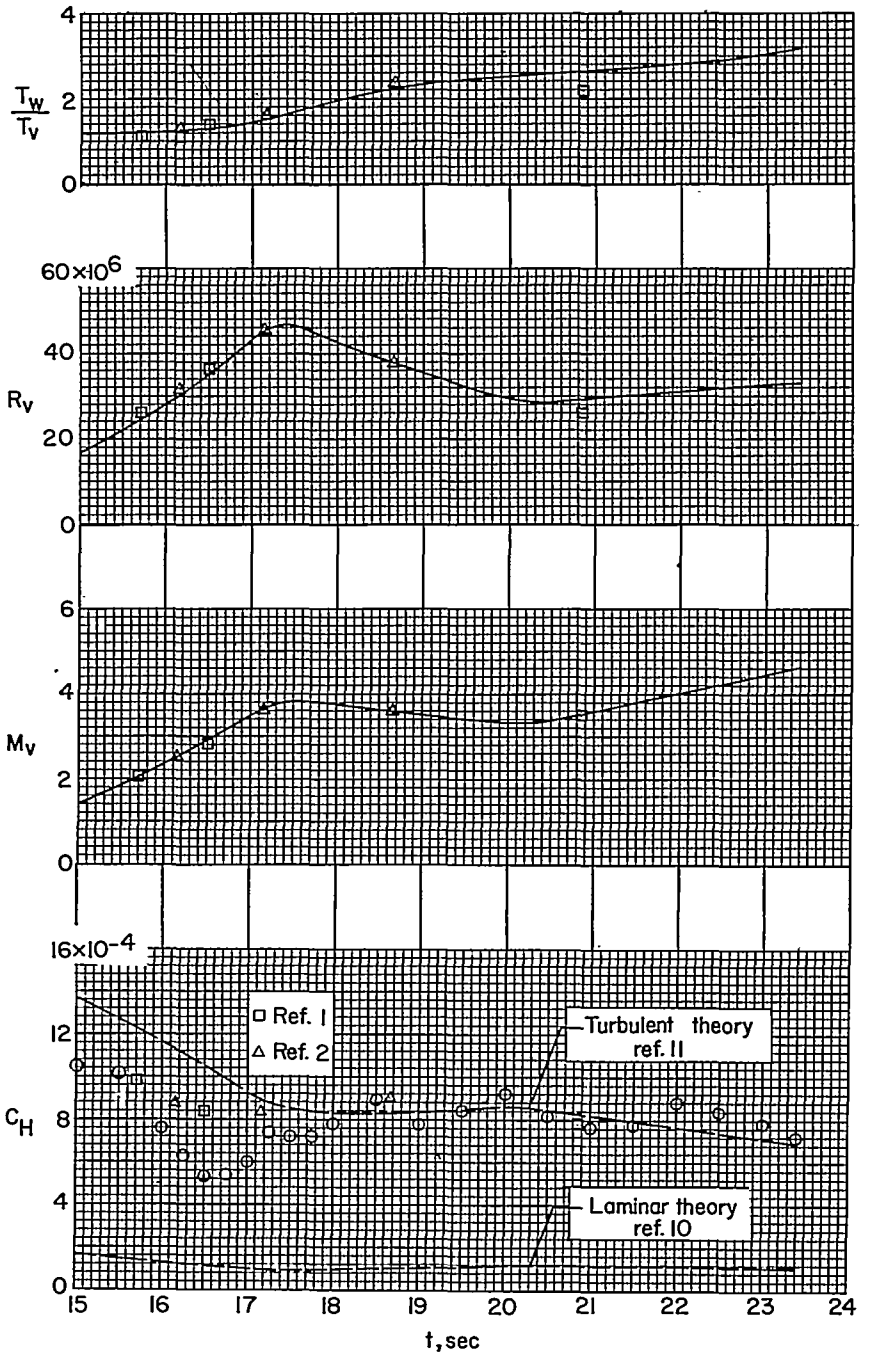

(i) Station 29.

Figure 5.- Concluded.

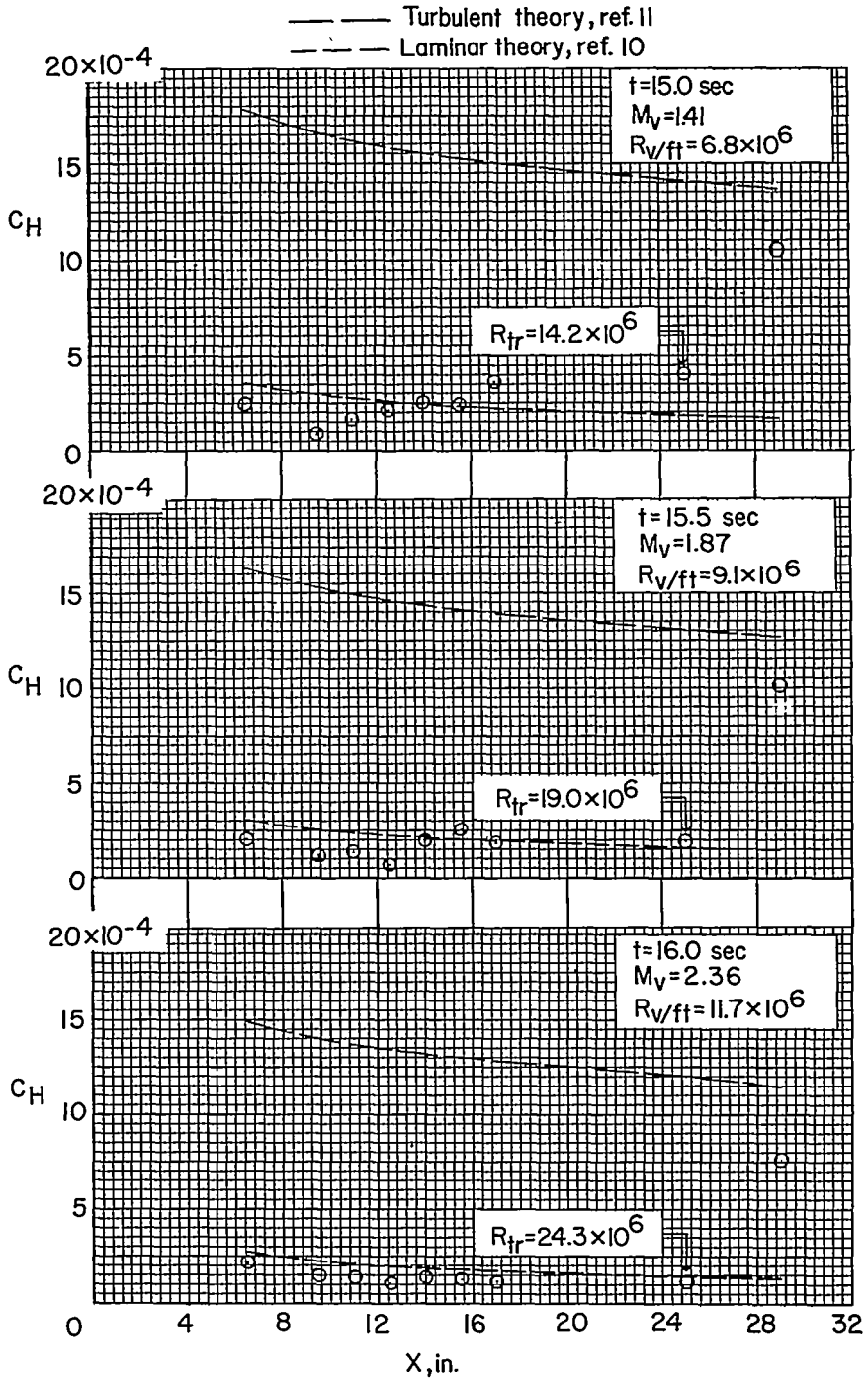

(a) Times 15.0, 15.5, and 16.0 seconds.

Figure 6.- Distribution of C_H along the nose.

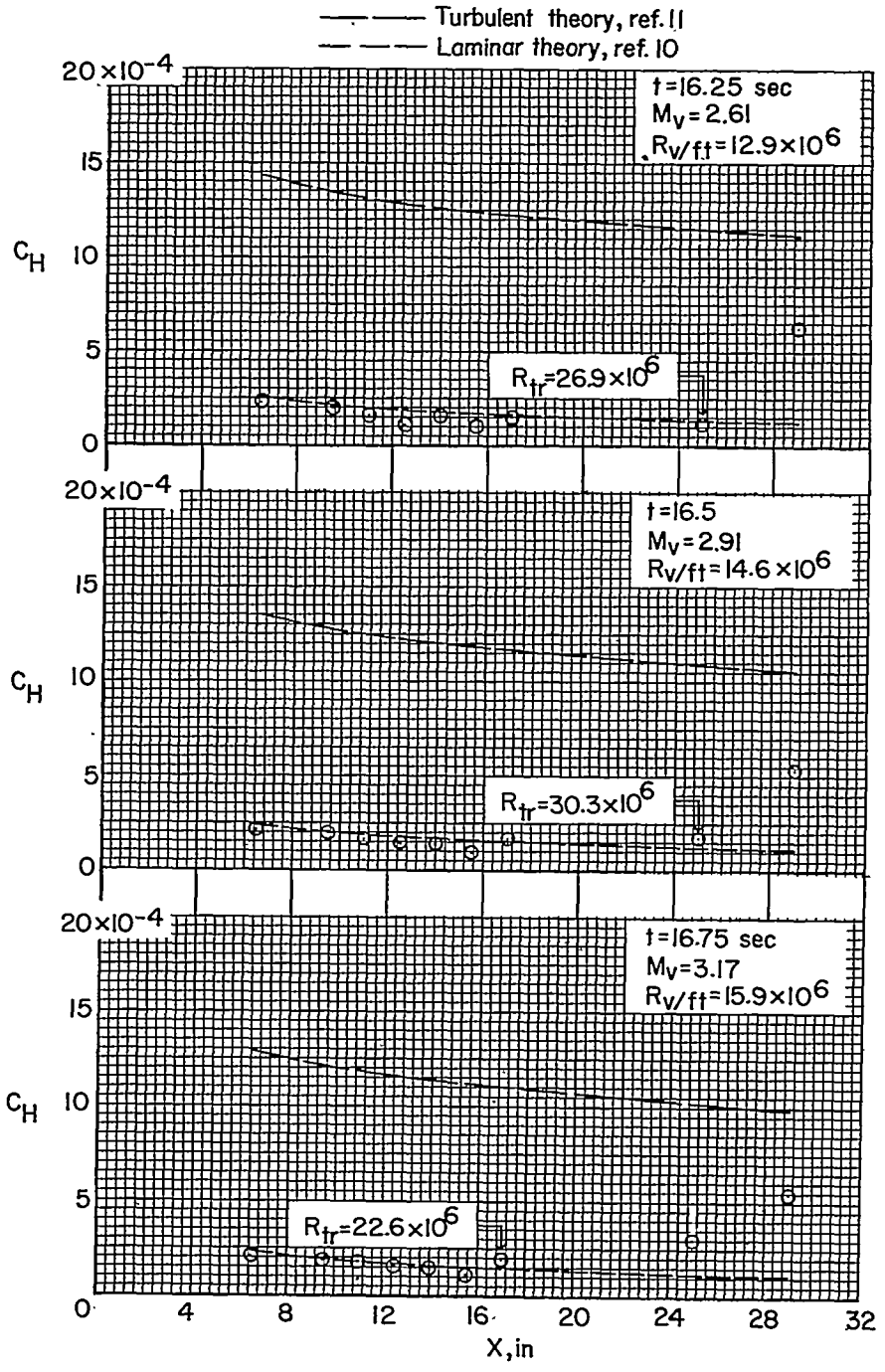

(b) Times 16.25, 16.5, and 16.75 seconds.

Figure 6.- Continued.

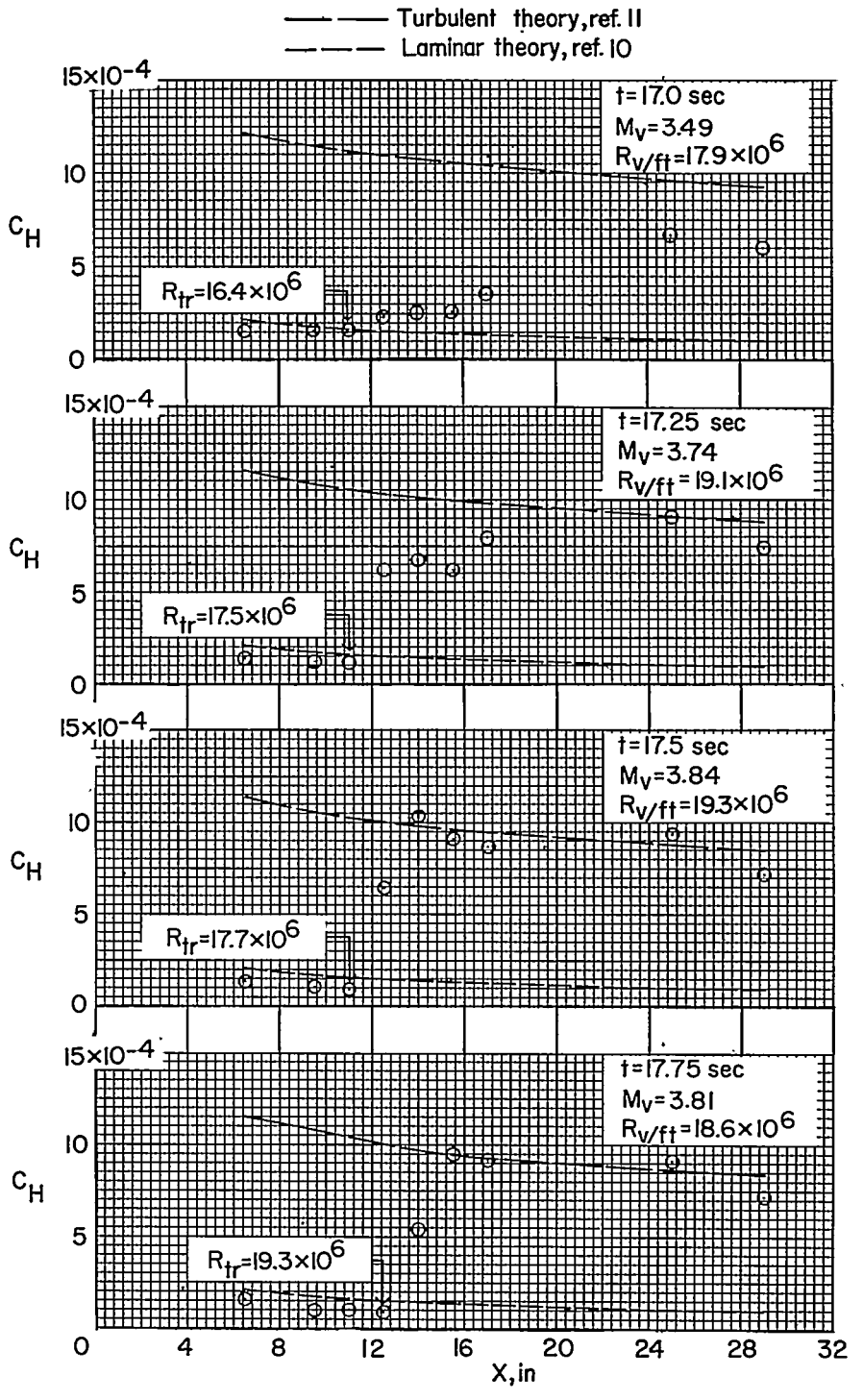

(c) Times 17.0, 17.25, 17.5, and 17.75 seconds.

Figure 6.- Continued.

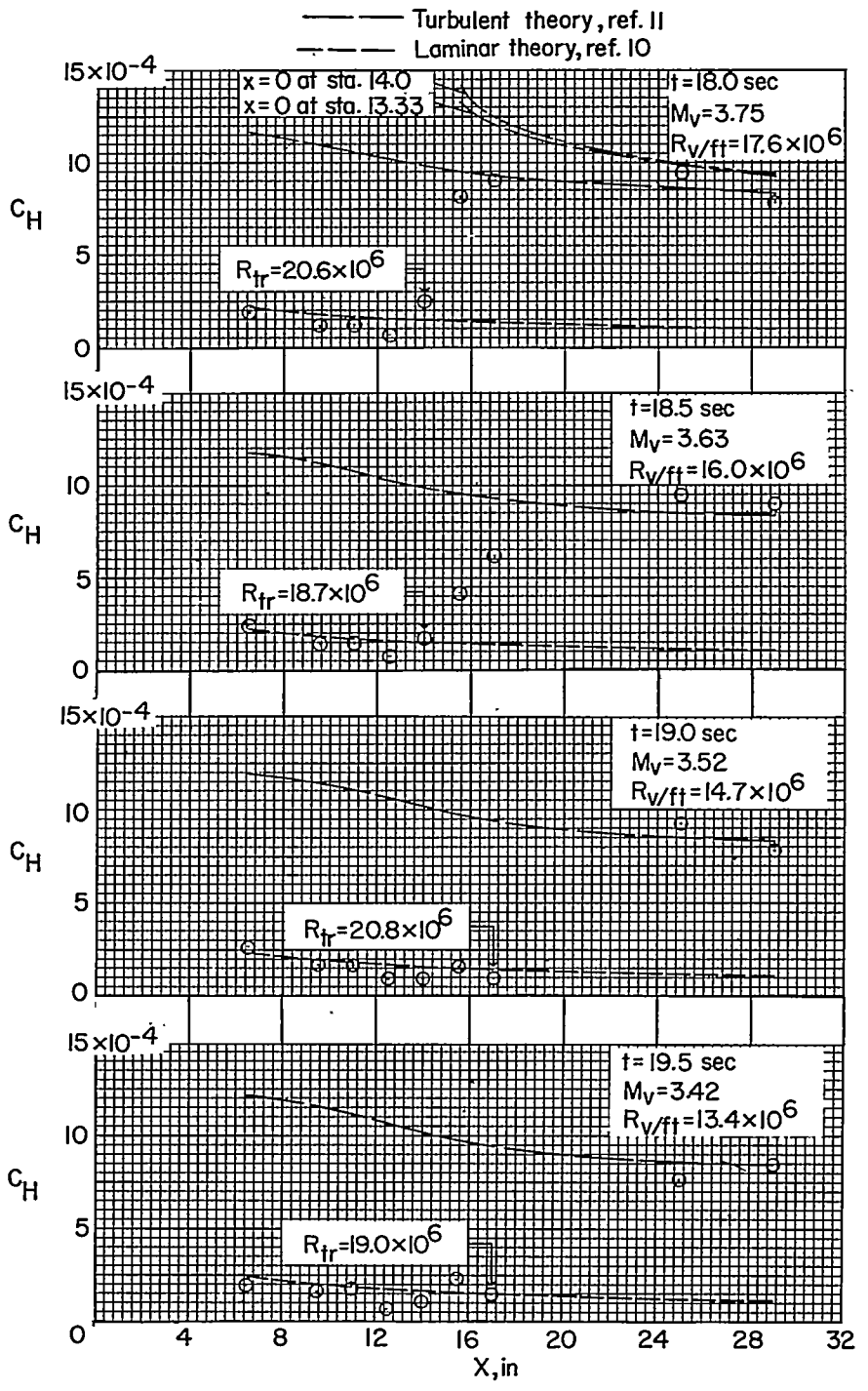

(d) Times 18.0, 18.5, 19.0, and 19.5 seconds.

Figure 6.- Continued.

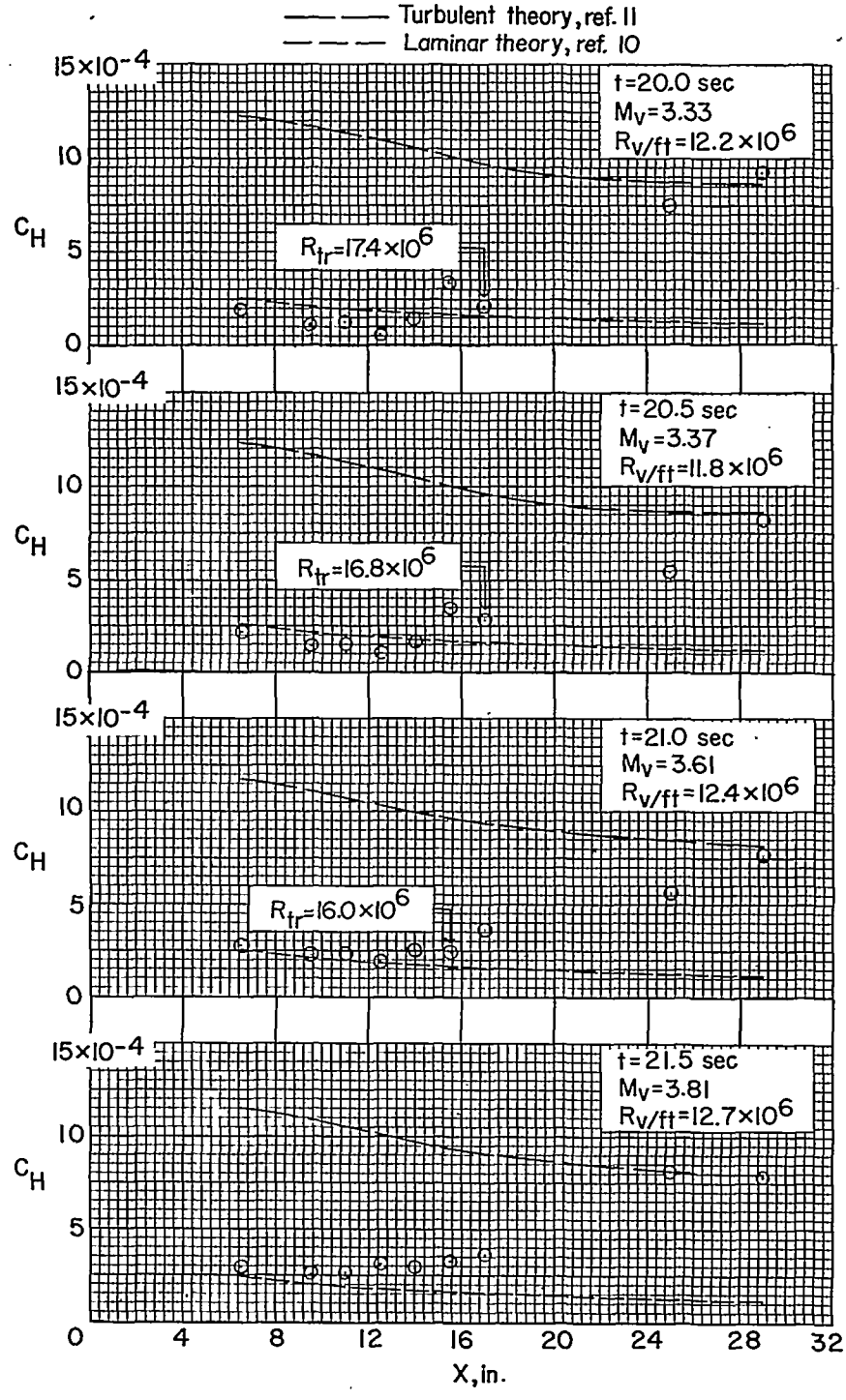

(e) Times 20.0, 20.5, 21.0, and 21.5 seconds.

Figure 6.- Continued.

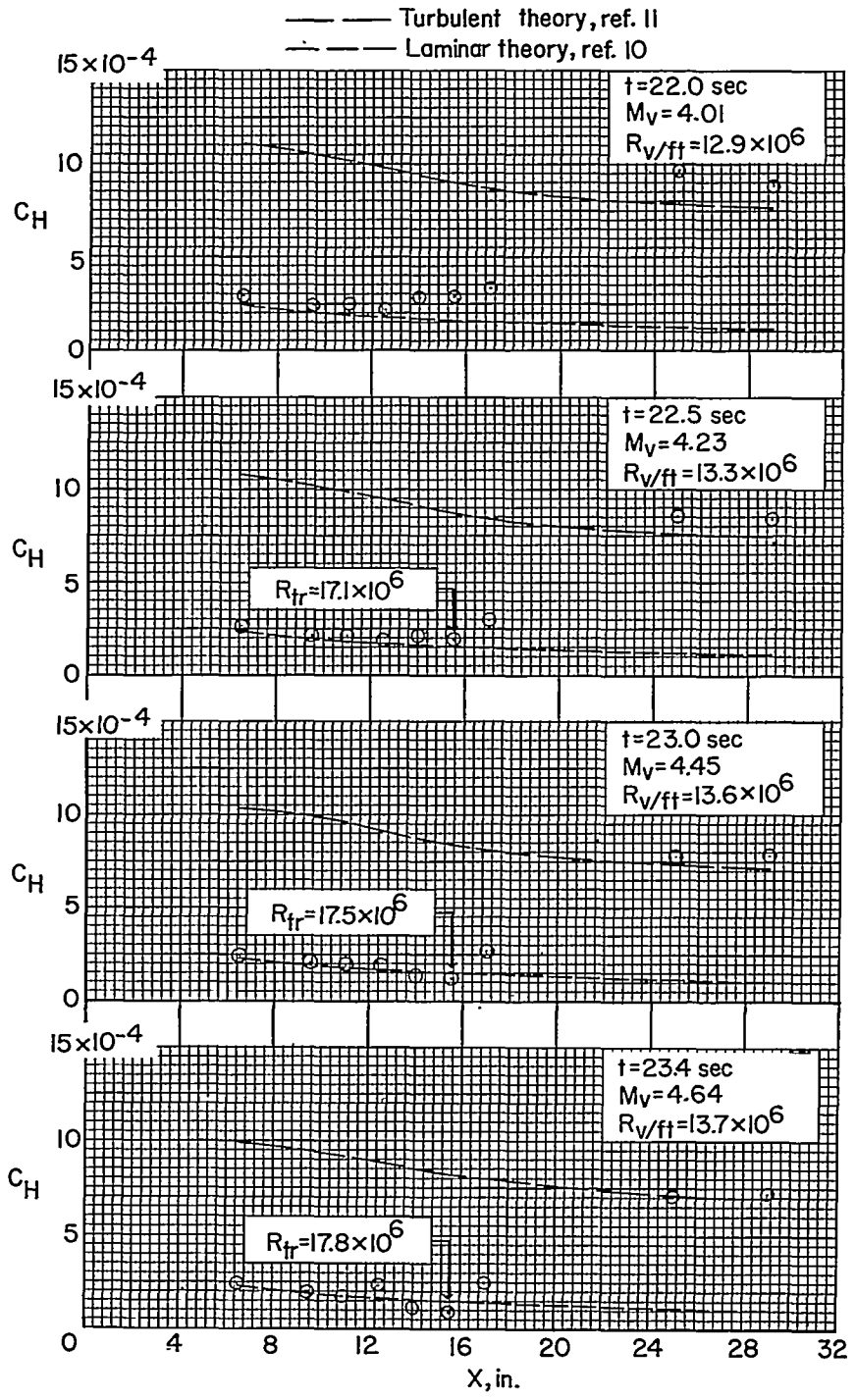

(f) Times 22.0, 22.5, 23.0, and 23.4 seconds.

Figure 6.- Concluded.

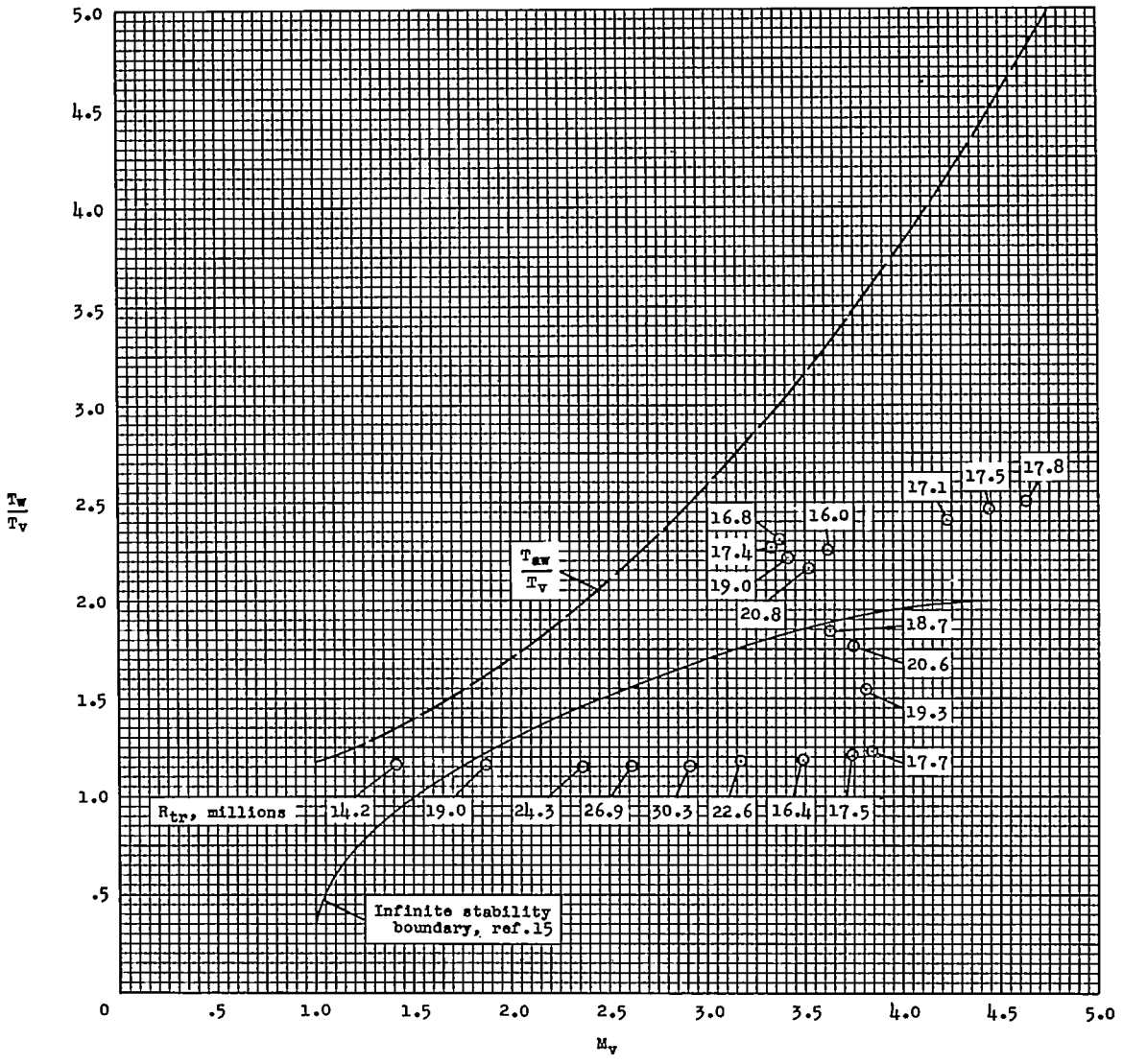

Figure 7.- Mach number and temperature-ratio conditions for measured transition Reynolds numbers.

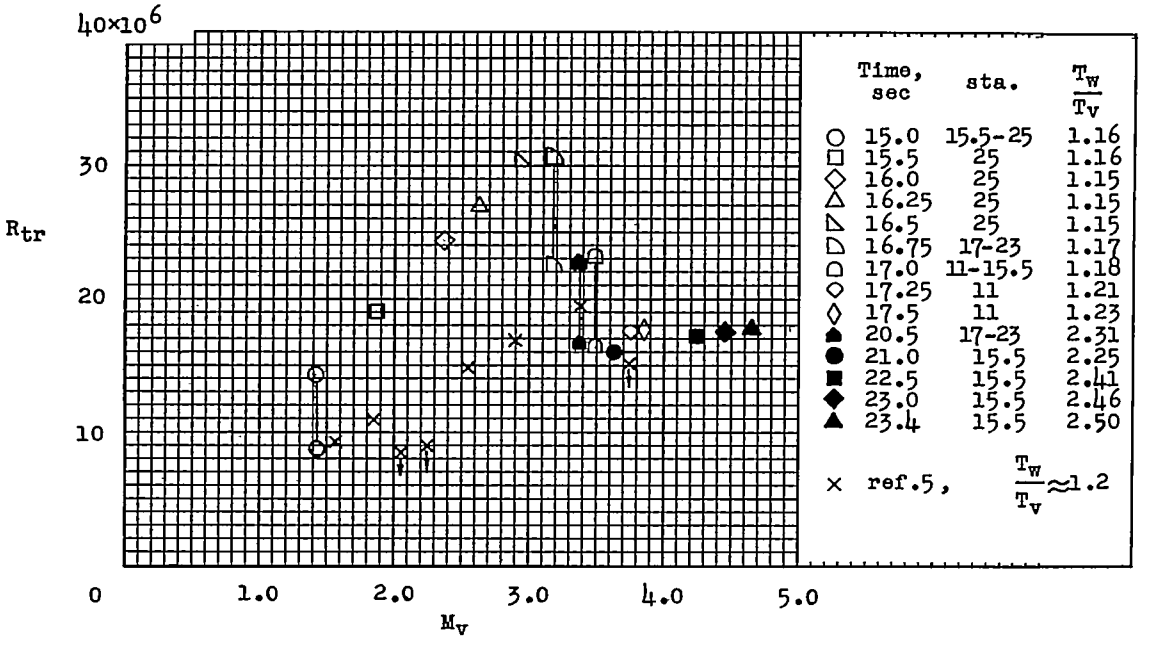

(a) R_{tr} as a function of Mach number.

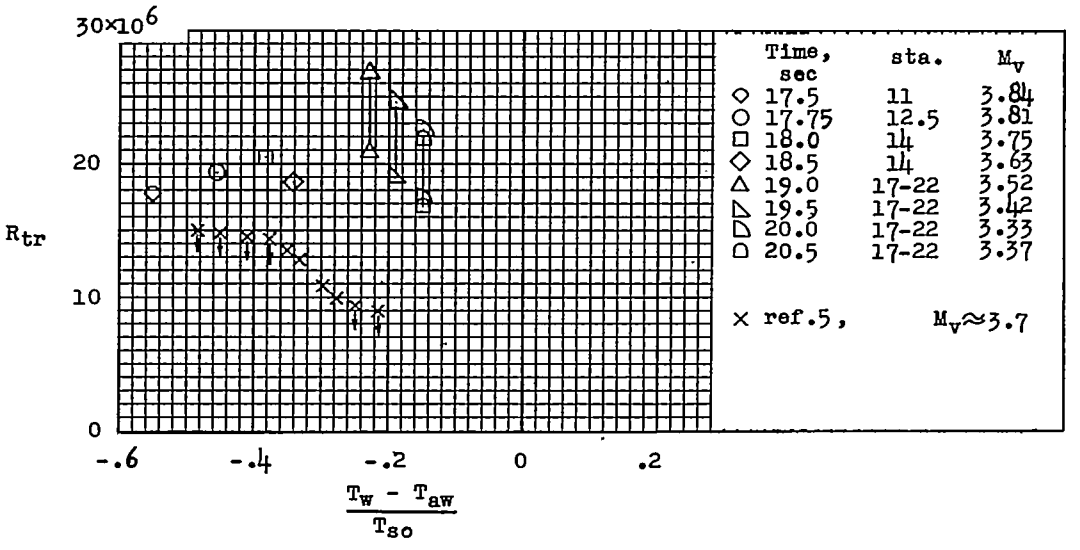

(b) R_{tr} as a function of $\frac{T_w - T_{aw}}{T_{so}}$.

Figure 8.- Experimental transition Reynolds numbers.

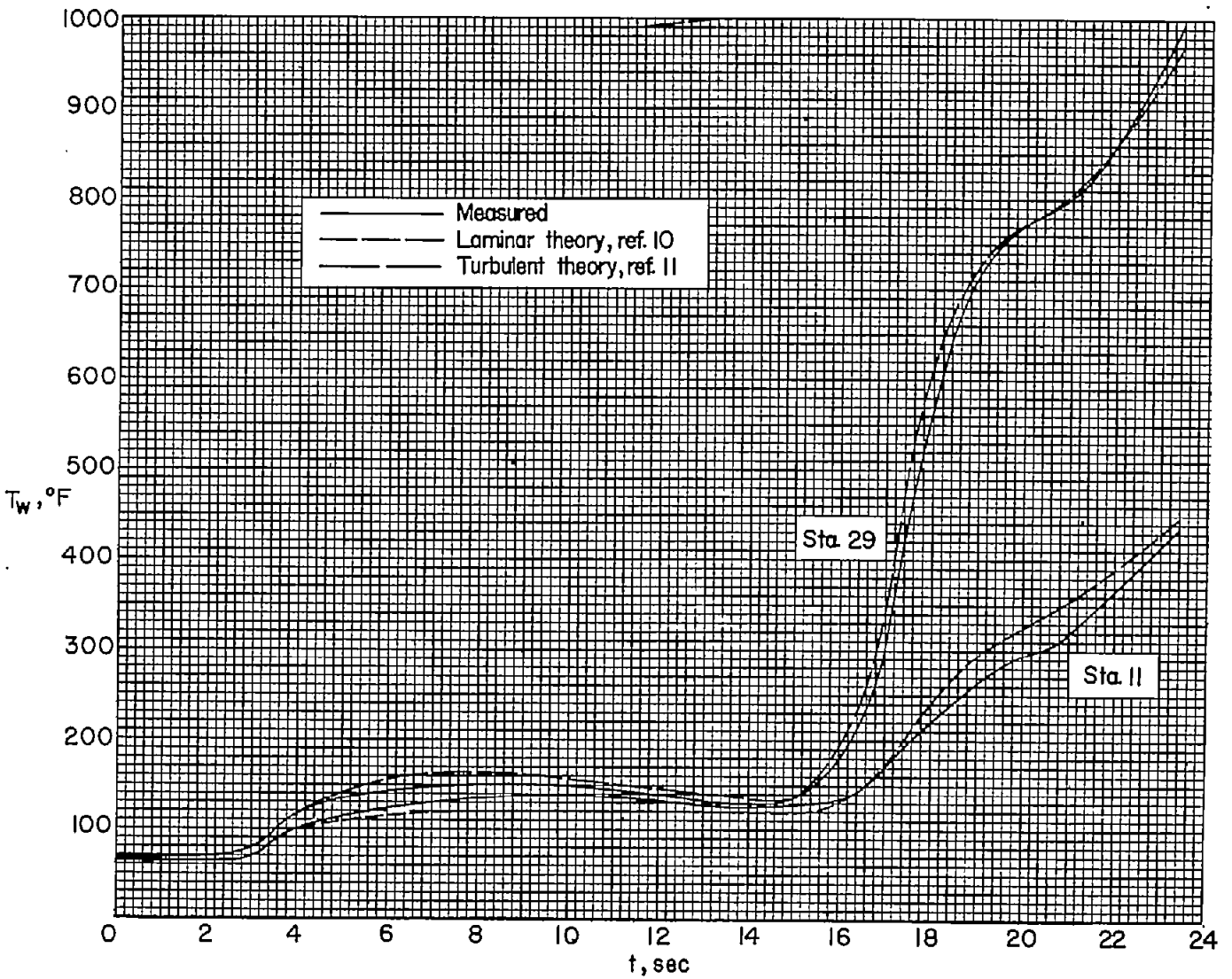

Figure 9.- Computed skin temperatures.

NACA - Langley Field, Va.

CONFIDENTIAL